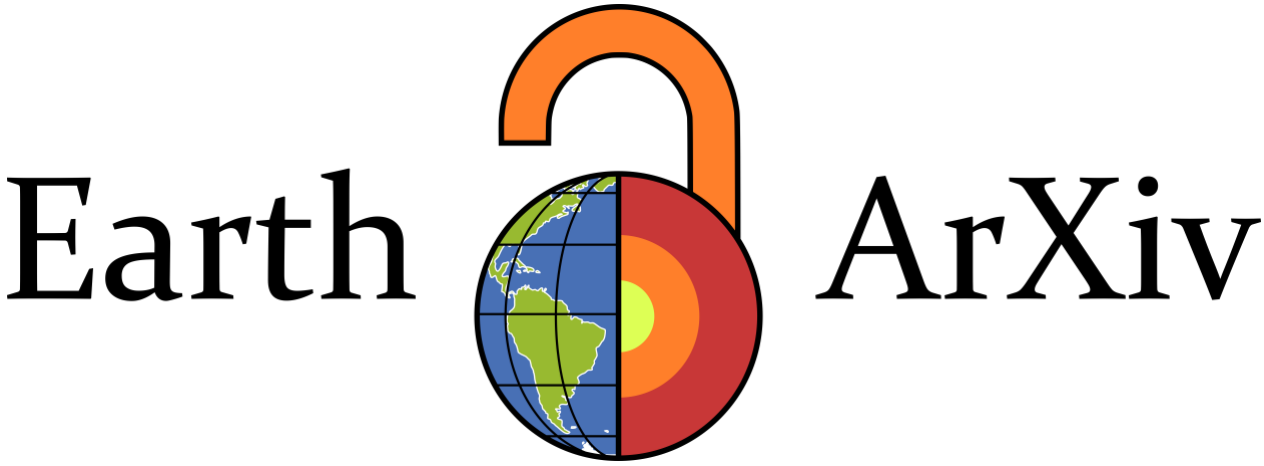

Future Sea Ice-Ocean and Biological Productivity Changes in the North Water Polynya Region under Policy Relevant Warming Levels

Jed E. Lenetsky,[a] Alexandra Jahn,[a] Patrick Ugrinow,[a] Christopher Wyburn-Powell,[a] Rajan Patel,[a] Hannah Zanowski,[b]

[a] *Department of Atmospheric and Oceanic Sciences and Institute of Arctic and Alpine Research, University of Colorado - Boulder, Boulder, Colorado, USA*

[b] *Department of Atmospheric and Oceanic Sciences, University of Wisconsin-Madison, Madison, Wisconsin, USA*

Corresponding author: Jed E. Lenetsky, jed.lenetsky@colorado.edu

ABSTRACT: The North Water Polynya (NOW) is one of the most productive biological regions in the Arctic with high importance to Inuit and Greenlandic communities. To provide insights into the potential changes of this region as global temperatures rise, we investigated the sea ice, and physical and biological oceanic responses of the NOW to low (2°C) and high (>3.5 °C) levels of warming using the Community Earth System Model version 1. As global temperatures increase, sea ice production decreases, spring open water area increases, and summer open water areas in the NOW region connect with open water in central Baffin Bay earlier in the melt season. These sea ice changes contribute to increased stratification, which in turn, leads to increased concentrations of nutrient-rich West Greenland Irminger Waters at depth while decreasing surface nutrient concentrations. At low warming levels in the eastern NOW region, warmer water temperatures increase phytoplankton growth rates despite the decrease in surface nutrients, leading to an increase in peak primary production relative to the historical period. In contrast, for high warming in both the eastern and western NOW regions, biological primary production decreases, despite the warmer water temperatures, because increased stratification and decreased surface nutrient concentrations limit phytoplankton production. For all assessed warming levels, changing phytoplankton community composition drives a loss of ecosystem productivity at higher trophic levels. Internal variability plays a negligible role in driving these future sea ice and ocean changes, highlighting the importance of limiting further global temperature increases in order to avoid large changes to the NOW ecosystem.

SIGNIFICANCE STATEMENT: The North Water Polynya (NOW) is one of the most productive biological regions in the Arctic with high importance to Inuit and Greenlandic communities. In this paper, we explore how sea ice, and physical and biological ocean conditions will change under low (2°C) and high (>3.5 °C) levels of global warming.

1. Introduction

The North Water Polynya (NOW) is one of the largest and most productive regularly occurring polynyas in the Arctic (Hastrup et al. 2018; Harning et al. 2023). Polynyas are defined as ocean regions of persistently thin or low concentration sea ice cover and are characterized by increased sunlight availability, vertical mixing, and nutrients (Marchese et al. 2017). In the NOW, located in Northern Baffin Bay between northwestern Greenland and the Canadian Arctic Archipelago, large and early phyotoplankton blooms help support key Arctic species such as walrus, polar bears, bearded seals, and beluga, bowehead, and narwhal whales (Odate et al. 2002; Tremblay et al. 2002; Heide-Jørgensen et al. 2013, 2016; Marchese et al. 2017). Additionally, little auk colonies transport nutrients onto land, supporting communities of Arctic land animals such as hares, geese, fox, reindeer, and muskox (Mosbech et al. 2018). Named the Pikialasorsuaq and Sarvarjuaq by the Greenlandic and Canadian Inuit, respectively, the NOW has served as important hunting grounds for Inuit and pre-Inuit communities for over four thousand years (Raghavan et al. 2014).

The NOW seasonally forms and is maintained by three processes: 1) the southward advection of sea ice away from the Nares Strait into central Baffin Bay due to northerly winds (Barber et al. 2001b; Dumont et al. 2010; Kwok 2007; Bi et al. 2019), 2) ocean mixing driven by latent heat fluxes and brine rejection from sea ice formation (Melling et al. 2001; Yao and Tang 2003; Mysak and Huang 1992), and 3) sensible heat fluxes from northerly winds and off-shore Ekman transports leading to the upwelling of warm, higher salinity, and nutrient-rich West Greenland Irminger Water (WGIW) along the West Greenland Coast (Melling et al. 2001; Burgers et al. 2023). These processes drive the active stage of the NOW, from October through April in which ice production in thin ice regions is ongoing (Tamura and Ohshima 2011; Ren et al. 2022), before leading into the post-polynya (inactive) stage from May until August in which areas of thin ice are the first to melt, leading to early open water areas and hot spots of biological activity surrounded by sea ice (Marchese et al. 2017). The Nares Strait ice arch aids the development of both the active and

inactive stages of the NOW, as it reduces the southward transport of thick, multiyear sea ice into Baffin Bay (Barber et al. 2001a; Dumont et al. 2009; Vincent 2019; Ren et al. 2022). Traditionally, the formation of the Nares Strait ice arch was viewed as a prerequisite for the formation of the polynya (e.g. Barber et al. 2001a), but recent years in which the ice arch never or only partially consolidated while the polynya nonetheless formed, have highlighted the importance that ocean mixing and sensible heat mechanisms play for the formation of the NOW (Moore et al. 2023, 2021; Vincent 2020; Howell et al. 2023). Changes in the Nares Strait ice arch have also coincided with reductions in fall sea ice concentration and growth in Northern Baffin Bay (Ballinger et al. 2022), as well as increasing polynya areas and the number of days when the polynya is present, especially in the fall and winter (Preußer et al. 2015; Stroeve and Notz 2018). Furthermore, annual phytoplankton bloom amplitude in the NOW may have declined between 1998 and 2014, associated with increased surface freshwater content from melting land ice and freshwater import from the Arctic Ocean (Marchese et al. 2017). However, if this observed change is a forced response due to warming or caused by interannual to multi-decadal variability is so far unclear (Marchese et al. 2017).

Throughout the late Holocene (~ 2200 to 1500 years ago), the NOW underwent a period of instability, influencing sea ice cover, stratification, and biological productivity (Koerner et al. 2021; Ribeiro et al. 2021). During this period, stronger northerly winds and storms destabilized the Nares Strait ice arch and increased the import of fresh Arctic surface waters into the NOW region (Koerner et al. 2021; Georgiadis et al. 2020). Increased sea ice import limited open water areas within the NOW region, reducing rates of sea ice formation and brine rejection, which, along with fresher surface waters, increased stratification. In turn, stably stratified surface waters impacted productivity by reducing the availability of nutrients in surface waters (Koerner et al. 2021). Changes in surface stratification also coincided with the increased northward penetration of warm, saline West Greenland Irminger Water (WGIW) into the NOW region, further increasing stratification (Jackson et al. 2021). These past changes in NOW oceanographic and biological regimes were substantial enough to influence the ability of societies to subsist in the region. Abandonment of human settlements 2000 years ago in the NOW region corresponds to this period of polynya instability (Ribeiro et al. 2021), and conversely, periods of human settlement in the NOW region correspond to periods of polynya stability (Grønnow 2016). Thus, understanding how

the NOW will change in the future is critical for the assessment and mitigation of climate change impacts in northern Baffin Bay.

Despite the ecological and societal importance of the NOW, projections for the NOW region were only recently examined for the 1981 to 2070 period (Buchart et al. 2022). It was shown that changes in future NOW conditions are likely to mirror those of past warmer climates with a less stable Nares Strait ice arch, and increased stratification from both increased surface freshwater fluxes and transports of WGIW via the Davis Strait (Buchart et al. 2022). These physical changes result in competing processes: larger northward transports of WGIW lead to increased nutrient availability below the mixed layer while increased stratification reduces the ability of those nutrients to reach the surface (Buchart et al. 2022). Even though this study is a substantial step forward in understanding the impact of climate change on the NOW, key questions remain, specifically in regards to projections of the polynya area and ice production, oceanic conditions after 2070, the impact of changes in the NOW on subregional spatial scales, the role of internal vs external climate variability, the potential impact of coupled air-sea ice-atmosphere interactions in the NOW, and the influence of changing phytoplankton production on higher trophic levels in the NOW ecosystem.

In the following, we address these outstanding questions about the NOW region, using the Community Earth System Model version 1 (CESM1). We do so in the context of policy-relevant specific warming levels as opposed to emissions pathways or time, following the approach taken in the most recent IPCC report (AR6, see Hausfather et al. 2022). In Section 3a we discuss model - observation agreement and sources of bias in the CESM1. In Section 3b, we explore the future evolution of sea ice conditions in the NOW under low warming and high warming levels, and in Section 3c and 3d, we explore oceanographic changes in the NOW region, focusing on the spring and summer during the post-polynya (inactive) stage, in order to link sea ice changes with changes to physical, chemical, and biological ocean conditions. We demonstrate that, despite relatively homogeneous physical oceanographic responses to climate warming across the NOW region, the biological productivity response to climate warming is non-uniform and non-linear under warming, while the energy transfer to higher trophic levels is again relatively uniform, with a marked decrease under both warming levels.

2. Data and Methods

a. Climate Simulations

In order to understand future changes in the NOW region for different warming levels and in the context of internal variability, we use model output from different ensemble simulations with the fully coupled CESM1-CAM5 at a nominally 1° resolution (Hurrell et al. 2013). Specifically, we use model output from the CESM1-LE (Kay et al. 2015) as well as one of the low-warming ensembles that are branched from the CESM1-LE in 2006 (Sanderson et al. 2017). The CESM1-LE, with 40 members, uses RCP8.5 from 2006 to 2100 while the low warming simulation, with 11 members, use RCP8.5 from 2006 to 2016 before switching to a greenhouse gas forcing designed so that global temperatures stabilize below 2 °C for at least 20 years before the end of the century (see Sanderson et al. 2017, for further details on the low-warming ensembles). We here use CESM1 output instead of output from the newer CESM2 because of more realistic Arctic sea ice fields in CESM1 (DeRepentigny et al. 2020; DuVivier et al. 2020), as well as the availability of dedicated CESM1 simulations that limit global warming to 2 °C (Sanderson et al. 2017).

We assess two warming levels for the period 2070-200: a high warming level (>3.5°C, red lines on Figure 1) that uses standard CESM1-LE data (forced by RCP8.5), and a low warming level (<2°C, yellow lines on Figure 1). The simulated global temperature anomalies for these warming levels are calculated relative to 1850–1879 in the first ensemble member from the CESM1-LE. The historical period is defined as the 30 year period from January 1980 to December 2009, in the CESM1-LE and the observational sea ice data. Hereafter, the low warming level will be referred to as LOW, and the high warming level will be referred to as HIGH.

b. Polynya definitions

We defined the NOW region in Northern Baffin Bay from 74°N to 79°N and 280°E to 305°E (see red box in Fig. 2). We use two different diagnostics to assess polynya changes within this region: ice production, based on ice growth during the fall and winter active stage (Tamura and Ohshima 2011; Ren et al. 2022), and extent of open water (polynya area), based on sea ice concentration during the summer inactive stage (Preußer et al. 2015). During the active stage, ice production is calculated as the combined monthly ice production (km^3) across both frazil and non-frazil ice categories within the CESM1 sea ice model.

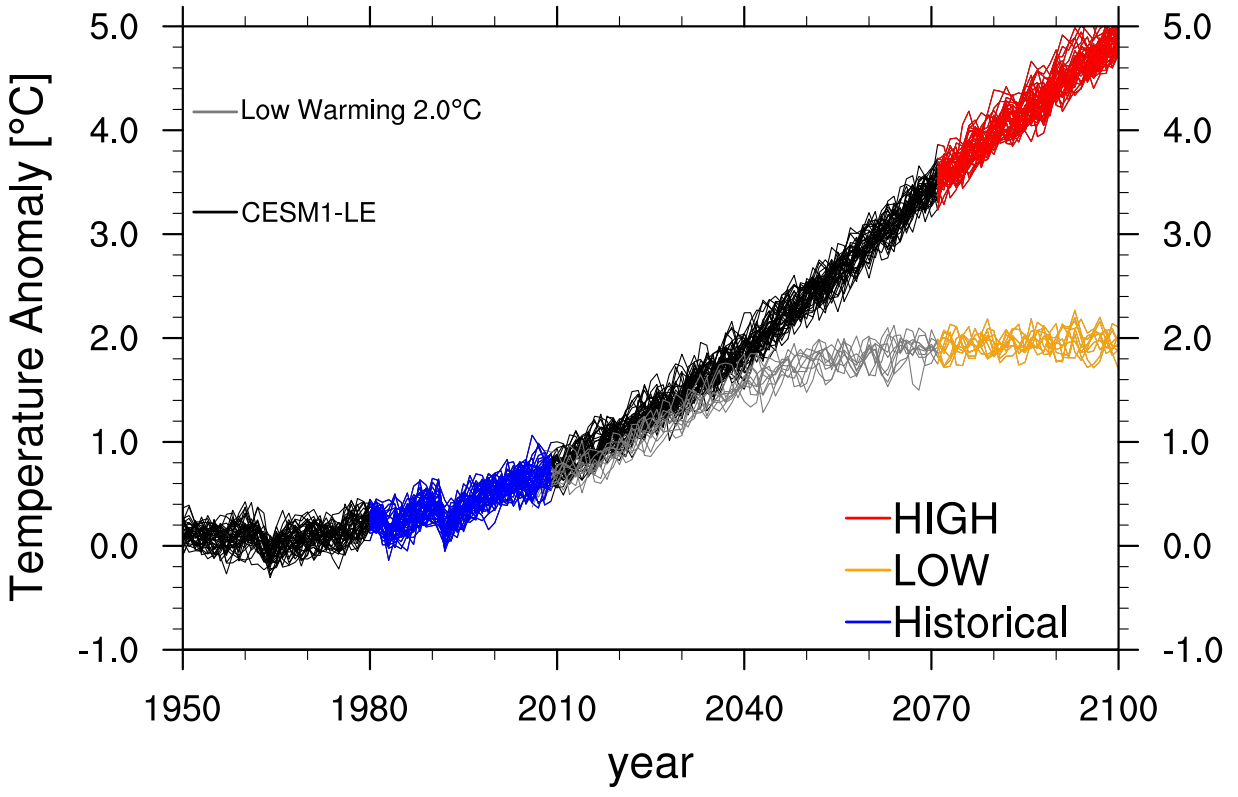

FIG. 1: Temperature anomalies relative to 1850-1879 from member 1 of the CESM1-LE (Kay et al. 2015) from the simulations used. In black, the CESM1-LE, and in grey the Low Warming Ensemble for 2°C (Sanderson et al. 2017). The periods from these simulations that are used are shown in blue for the historical period, orange for low warming (LOW), and red for high warming (HIGH). Details on the global temperature anomalies for the different warming levels can be found in Table S1.

For the post-polynya stage, the polynya area is calculated as the sum of the area of grid cells within the polynya region with a sea ice concentration (SIC) below 70%, which we used as a threshold for the presence of open water, following Preußer et al. (2015). Note that model resolution and SIC threshold may influence the post-polynya area (Landrum et al. 2024). Following previous studies that differentiate between the presence of a polynya and continuous open water in northern Baffin Bay (e.g. Dunbar and Dunbar 1972; Barber et al. 2001b), we define a second region in eastern, central Baffin Bay from 72°N to 74°N and 295°E to 305°E (yellow box in Fig. 2). When the average SIC there is less than 50% in this southern region, the NOW is considered to be connected to the Baffin Bay open water region, with no polynya present (i.e., polynya area is 0). Conversely, when the majority (>50%) of this southern region is covered in sea ice, any open water within the

NOW region is considered to be closed and isolated from open water further south, and thus part of the polynya. The choice of this southern SIC threshold does not affect the polynya in the winter and spring, but does affect the timing and magnitude of the polynya's peak area and its dissipation and formation in the summer and fall (Fig. S1). Note that the use of this second region has the effect of lowering polynya area climatologies by averaging areas of open water when the polynya is present with areas of zero when the polynya is not present (see July in Fig. 3b).

In order to understand the spatial variability of changing ocean conditions within the NOW region, we also define an ocean section across the NOW (76.2°N, 280 - 289.5 °E) and examine ecological changes at one eastern location (76.2°N, 289°E) and one western location (76.5°N, 283°E) along the section (see Fig 2). The results presented are insensitive to the exact choice of the eastern and western locations.

To assess the ability of the CESM1 to simulate the present-day NOW polynya during the inactive stage, polynya areas calculated from the historical simulation are compared to observed polynya areas calculated from monthly NOAA/NSIDC Climate Data Record of Passive Microwave Sea Ice Concentration (SIC), version 4 (Meier et al. 2021).

c. Ice fluxes

In order to assess the contribution of sea ice from the central Arctic Ocean on sea ice conditions in the NOW, we define the Nares Strait ice area flux (IAF) as:

$$IAF = \int_L (SIC * V_{ice}) dL \tag{1}$$

where SIC is the sea ice concentration, V_{ice} is the meridional sea ice velocity, orthoginally crossing the Nares Strait northern gateway at 292.2 - 295.6°E and 82.6°N (Fig. 2), and L is the length of the gateway (127 km; Fig 2). The results presented are insensitive to both the location of the gateway in northern versus southern Nares Strait. We also compare simulated sea ice area fluxes during the historical period with satellite observations for 1997-2009 (Kwok et al. 2010) and 2016-2019 (Moore et al. 2021) based on available datasets.

We also assess solid freshwater fluxes as the sum of sea ice and snow on sea ice freshwater equivalents through the Nares Strait and southern NOW (74°N; 285:300°E) as

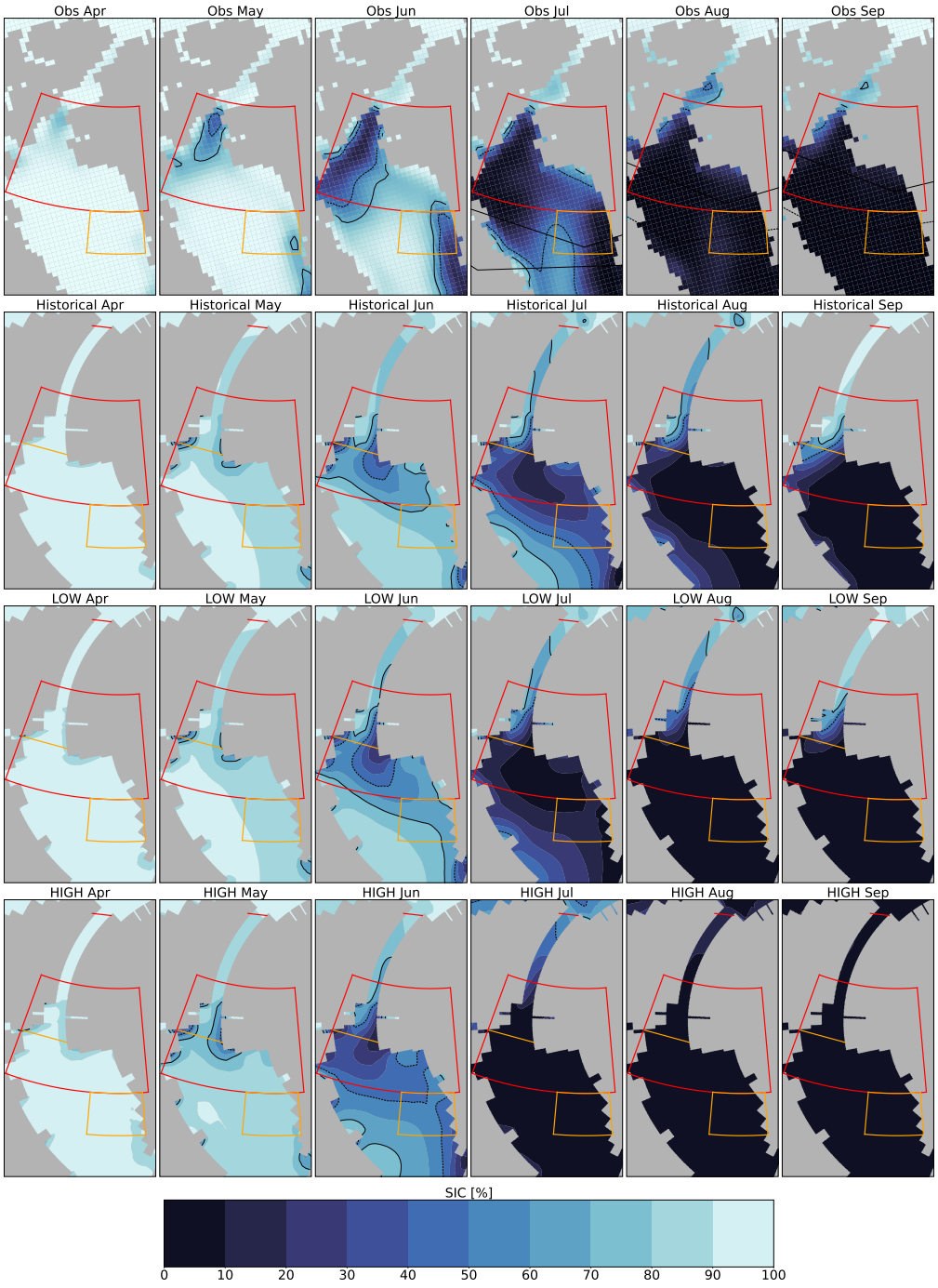

FIG. 2: Observational and ensemble mean May, June, July, August, September, and October sea ice concentrations (SIC) in Northern Baffin Bay from the NSIDC observational passive microwave record (Meier et al. 2021) for the historical period 1980-2009 (first row), and the CESM1 for the historical period (second row), LOW (third row), and HIGH (bottom row). The North Water Polynya (NOW) region is outlined in red and the southern region is outlined in yellow. The 70% SIC contour is outlined in a black solid line and the 50% SIC contour is outline in a black dashed line. The approximate location of the northern Nares Strait gateway is shown in red and location of the NOW ocean cross section used in Figs. 8 & 9 is shown in orange.

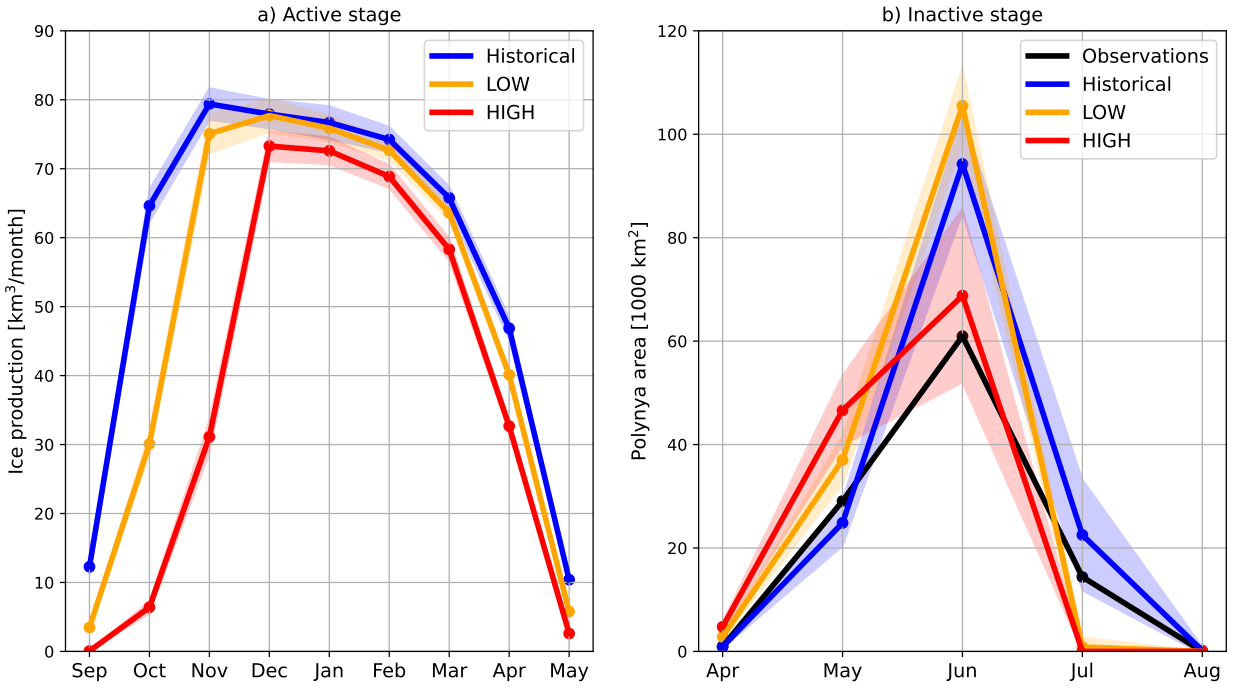

FIG. 3: Changing seasonal cycle of polynya ice production during the active stage (a) and and polynya area during the inactive stage (b), from observations (inactive only; 1980-2009; black), CESM1-LE historical period(1980-2009; blue), LOW (yellow), and HIGH (red). Shading indicates ± 1-standard deviation from the ensemble mean.

$$FFW_{solid} = \frac{\rho_{ice}}{\rho_{fw}} \int_H \int_L \frac{S_{ref} - S_{ice}}{S_{ref}} (SIC * V_{ice}) dLdH + \frac{\rho_{snow}}{\rho_{fw}} \int_H \int_L (SIC * V_{ice}) dLdH \quad (2)$$

where H is the thickness of the layer, S_{ref} is reference salinity (34.8 g/kg), S_{ice} is sea ice salinity (4 g/kg), and ρ_{snow}, and ρ_{fw} are the densities of sea ice (917 kg/m^3), snow (330 kg/m^3), and pure freshwater (1000 kg/m^3) respectively.

d. Assessment of stratification

In order to quantify vertical changes to ocean density in the NOW under different warming levels, which can influence nutrient availability and biological productivity, we define buoyancy content (B; Schmidt and Send 2007) as

$$B = -\frac{g}{\rho_0} \int_0^h [\rho(z) - \rho(h)] dz, \quad (3)$$

where g is gravitation acceleration, ρ_0 is reference density of 1025 kg/m^3, and $\rho(h)$ is the potential density at the base of the ocean layer with thickness h. B, similarly to other metrics such as available potential energy (Gjelstrup and Stedmon 2024; Polyakov et al. 2018), is a vertically integrated measure of stratification, and represents the energy required to remove vertical density gradients and fully mix the water column from the surface to depth h. Furthermore, following Schmidt and Send (2007), we can use the linearized equation of state, $\rho = \rho_0(1 - \alpha\Delta T + \beta\Delta S)$, to estimate the relative contributions of temperature and salinity to B:

$$B \approx B_T + B_S \tag{4}$$

$$B_T = g\alpha \int_0^h [\Theta(z) - \Theta(h)]dz \tag{5}$$

$$B_S = -g\beta \int_0^h [S_A(z) - S_A(h)]dz \tag{6}$$

where Θ is the conservative temperature, S_A is the absolute salinity, and α and β are the thermal expansion and haline contraction coefficients respectively. In the following, we calculate B, B_T, and B_S over the upper 55 and 155 meters of the water column in order to assess both near surface and deeper changes to stratification. The results presented are insensitive to the exact choice of h.

e. Simulated biogeochemistry

The CESM1 simulations used in this study are all run with biogeochemistry from the fully-coupled Biogeochemical Elemental Cycle (BEC) model (Moore et al. 2001, 2004, 2013). The BEC model includes key elements for oceanic chemistry (C, O, N, P, Fe, Si) in addition to multiple phytoplankton functional groups (diatoms, small phytoplankton, diazotrophs) and zooplankton. Note that diazotrophs are not considered in this study as they are not present in polar regions even under HIGH scenarios (Krumhardt et al. 2022). As a result, Net Primary Productivity (NPP) is defined as the sum of the net production of organic matter from photosynthesis across both small phytoplankton and diatoms. Assessments of NPP in the NOW are important to assess the impact of climate change in the NOW on the carbon cycle. Together with phytoplankton community composition, NPP also provides insights into changes in the base of the marine food web.

We diagnose nutrient availability using nitrate concentration because in northern Baffin Bay, nitrogen is the primary limiting nutrient for both diatom and small phytoplankton growth (Moore et al. 2013) and nitrate concentrations are two orders of magnitude larger than ammonium concentrations. For the biogiochemical variables assessed, fewer ensemble members than for the physical variables are available, as ocean biogeochemistry was corrupted in members 3–8 in the CESM1-LE (see the known issues on the CESM1-LE project website), which affects both the CESM1-LE and the low warming simulations that were initialized from the CESM1-LE. We also do not include member 1 of the CESM1-LE in analyses of biological productivity due to net primary production values being far outside the range of other members of the CESM1-LE during the historical period (for unknown reasons).

Diatom fraction (df), the proportion of net primary production (NPP) that is produced by diatoms (NPP_{diat}) versus small phytoplankton (NPP_{sp}), is given by

$$df = \frac{NPP_{diat}}{NPP_{diat} + NPP_{sp}}. \tag{7}$$

Ecosystem Trophic Efficiency (ETE) is the ratio of how much energy is available to higher trophic levels relative to total NPP. It provides information on impacts of NPP and community composition changes on higher tropic levels. Following Krumhardt et al. (2022), we define ETE as:

$$ETE = \frac{df * F_z * E^{L-2.1}}{NPP}. \tag{8}$$

Here, we assess ETE for pelagic tropic level 3 (i.e., the species feeding on zooplankton), where F_z is the vertically integrated zooplankton production, $L = 3$ is the trophic level, and $E = 0.14$ is the food web trophic efficiency (Krumhardt et al. 2022). Here, $df * F_z$ is the mesozooplankton production (diatom fraction times zooplankton production), representing production by large zooplankton, which are more likely to be consumed by consumers at higher trophic levels than small zooplankton (Krumhardt et al. 2022; Stock et al. 2017).

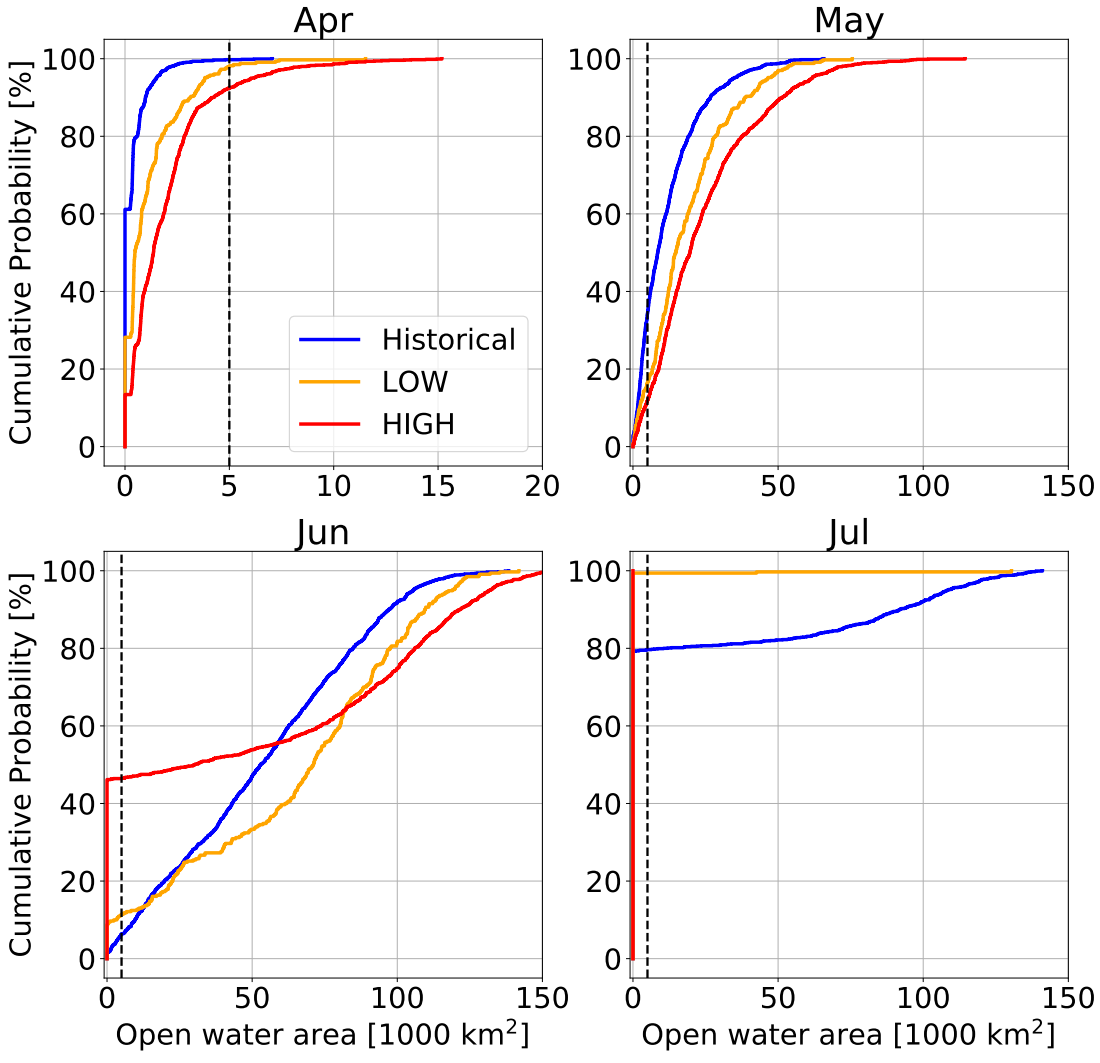

FIG. 4: Cumulative probability of open water areas [in 1000 km^2] from CESM1-LE historical period (1980-2009; blue), LOW (orange), and HIGH (red). The dashed black line shows the arbitrary threshold of 5000 km^2. Note the different x-axes on each of the panels, due to the different polynya areas for April compared to May through July.

3. Results

a. Modelled North Water Polynya over the historical period

The simulated seasonal cycles of the polynya diagnostics (ice production and area) are qualitatively very similar to the observed seasonal cycle over the historical period during all seasons

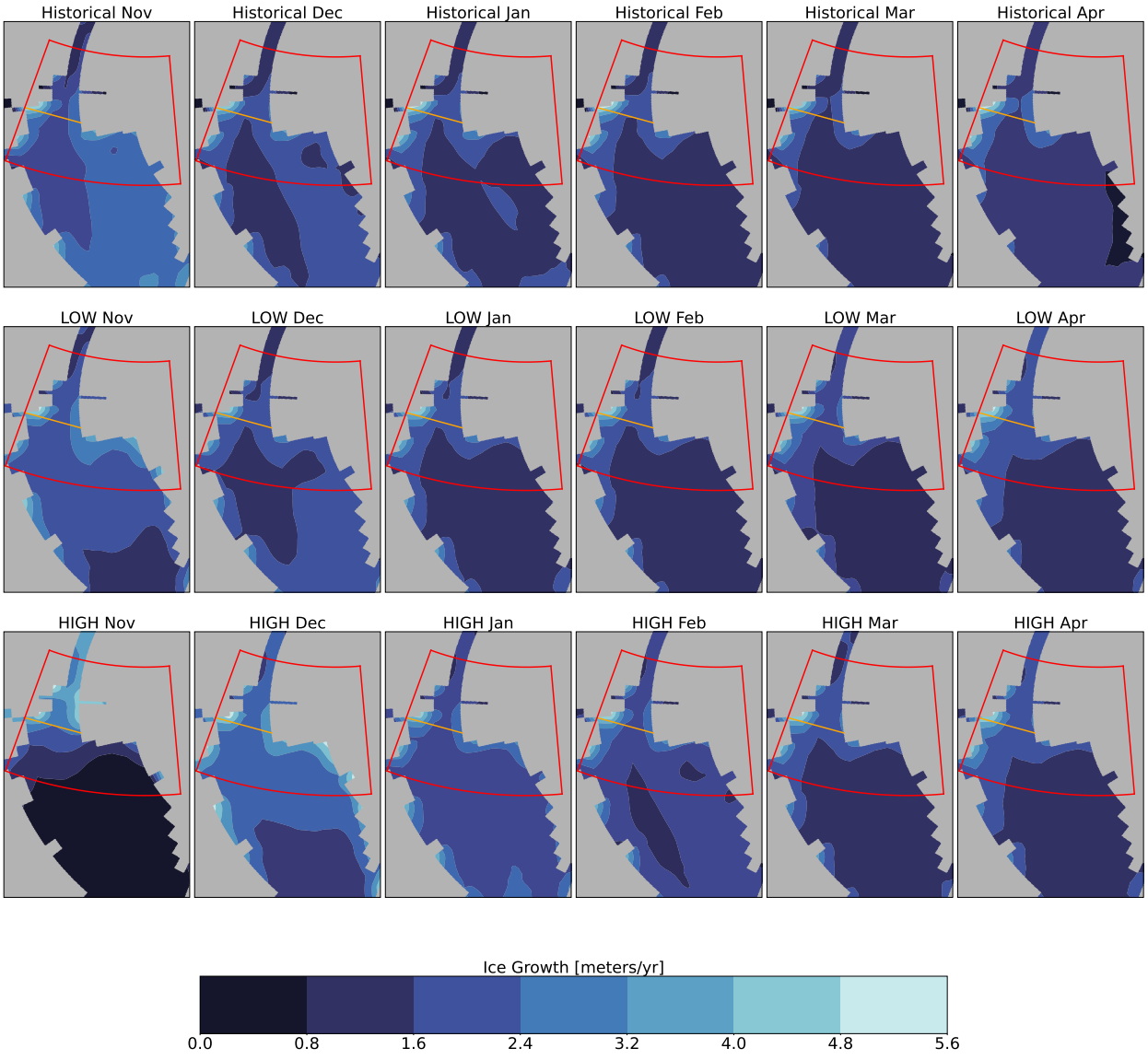

FIG. 5: Ensemble mean November, December, January, Fabruary, and April sea ice growth rates in Northern Baffin Bay the simulated historical period 1980-2009 (first row), LOW (second row), and HIGH (bottom row). The North Water Polynya (NOW) region is outlined in red and the location of the NOW ocean cross section used in Figs. 8 & 9 is shown in orange.

(Fig. 3), with the seasonal cycle of simulated sea ice production rates agreeing with observational estimates in terms of both regionally averaged magnitude and seasonal cycle (Tamura and Ohshima 2011; Ren et al. 2022). The active stage of the NOW begins in September when ice growth begins, peaking in November at $\sim$ 80 km^3/month of sea ice growth and slowly declining until May when ice growth ceases (Fig. 3a). In the inactive post-polynya stage from May to July, simulated polynya areas during the historical period agree quite well with satellite sea ice observations, except for

a substantially larger peak area in June (Fig. 3b). After the inactive polynya peaks in June, the seasonal retreat of sea ice in Baffin Bay begins to reduce SIC south of the NOW region, connecting the NOW to the open waters of northern and central Baffin Bay (Fig. 2). As a result, even though open water is still increasing in the NOW region in July (Fig S1), the 30-year average polynya area in July declines as the NOW ceases to be a polynya in several years and becomes open water instead (Fig 4). Thus, non-zero polynya areas less than the June peak in July reflect primarily internal variability in sea ice conditions south of the polynya, as opposed to changing sea ice conditions within the NOW region.

Despite the good agreement on the seasonal cycle of the polynya ice growth and area, the spatial ice growth and SIC in the NOW region in spring differs between the CESM1 and observations (Fig. 2 & 5). This difference is most likely primarily due to the absence of a Nares Strait sea ice arch in the CESM1, resulting in simulated historical ice area fluxes that have a different seasonal cycle and are larger than observed fluxes in the spring and summer over the 1997-2009 period (Fig. 6a; Kwok et al. 2010). The simulated seasonal cycle of Nares Strait sea ice fluxes over the historical period shows a late fall and winter minimum rather than a minimum in spring, and hence shows a much earlier increase in the simulated sea ice area fluxes after the seasonal minimum. Furthermore, the similarity in solid freshwater transports between Nares Strait and southern Baffin Bay (Fig. 6c-d), is in disagreement with observations that show that Nares Strait sea ice transports do not substantially contribute to sea ice transports in southern Baffin Bay (Howell et al. 2024). Despite high winter and spring sea ice concentrations (SIC > 85%), monthly mean sea ice velocities magnitudes in the Nares Strait are too large (> 0.1 cm/sec) to be considered slow pack ice according to Laliberté et al. (2018), suggesting that the ice arch would still be missing in CESM1 even with the inclusion of updated landfast ice parameterizations (e.g. Lemieux et al. 2016; Sterlin et al. 2024). As a result, we conclude that in the CESM1, large Nares Strait sea ice areas fluxes are due to a combination of the coarse model resolution that is unable to resolve the narrow passages of the Nares Strait interior, and weak internal ice stresses (despite high sea ice concentrations) that are unable to adequately resist wind stress (Dumont et al. 2009). Note that in higher resolution CESM1 simulations, Nares Strait ice area fluxes still show an opposite seasonal cycle compared to Kwok et al. (2010), peaking in spring instead of fall (Fol et al. 2025), suggesting that model resolution alone cannot explain biases in ice area transports.

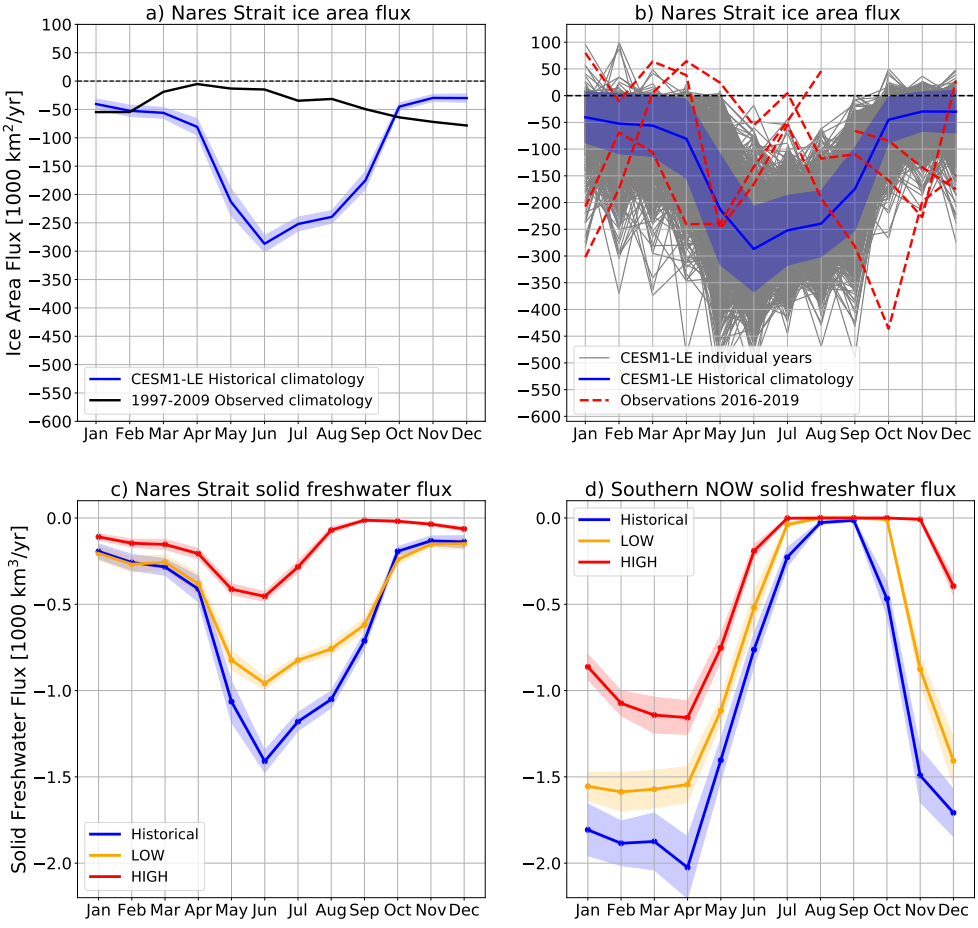

FIG. 6: Seasonal cycles of sea ice area and solid freshwater fluxes in the NOW region. Negative values indicate southward fluxes. Panel a) shows the observed climatology of ice area fluxes from 1997-2009 across the northern Nares Strait (Kwok et al. 2010) in black, and the simulated climatology over the CESM1-LE historical period (1980-2009). Blue shading indicates ± 1-standard deviation from the ensemble mean climatology. Panel b) again shows the simulated ice area flux climatology in blue over the historical period, along with individual annual cycles for each year and member from the CESM1-LE historical period in grey. Blue shading indicates ± 1-standard deviation of annual cycles across all years and members. Available years of recently observed ice area fluxes from years (2016-2019; Moore et al. 2021) when the ice arch was less stable are shown in red dashed lines. Observational uncertainties are small at approximately 4.4 1000 km^2/yr (Moore et al. 2021). Panels c) and d) show solid freshwater fluxes through Nares Strait (c) and southern NOW region (d) for historical (blue), LOW (orange), and HIGH (red), with shading indicating ± 1-standard deviation from the ensemble mean climatology.

The impact of the differences in the simulated and observed Nares Strait sea ice flux is most apparent on sea ice growth rates during the fall and winter, when ice growth rates are substantially reduced compared to observations by ~15 meters/year and regions of sea ice growth are only present on the eastern and western margins of the NOW south of Nares Strait (Fig. 5), as opposed

to in the central channel as seen in observations (Tamura and Ohshima 2011; Ren et al. 2022). These discrepancies in ice growth rate and spatial pattern are consistent with the steady inflow of pack ice through Nares Strait, insulating the ocean surface and limiting the exchange of turbulent heat with the atmosphere, which in turn, inhibits sea ice growth (Fig. S2; Mysak and Huang 1992; Melling et al. 2001; Yao and Tang 2003). Key differences are also present in the April and May SIC (Fig. 2), when the observations show approximately 10-30% lower SIC and a polynya forming south of Nares Strait while the simulated polynya is confined to the coastlines. This spatial difference is due to ice being advected by northerly winds to the south from away from Greenland and Ellesmere Island, as opposed to away from an ice arch in the central channel. In June, the much larger simulated Nares Strait sea ice area flux in the CESM1 is also clearly apparent in the spatial SIC, with a relatively high SIC tongue extending into northern Baffin Bay in the CESM1 (Fig. 2). Nonetheless, the CESM1 simulates a large polynya across the NOW region in June, in agreement with data from more recent years that show that the NOW polynya formed despite no Nares Strait ice-arch forming (Moore et al. 2021, 2023). In terms of the effect of biased ice area fluxes on future projections of open water area and ice production in the NOW region, we expect the lack of an ice-arch to have less of an effect than for historical conditions, as the recent frequent breakdowns or failures to form an ice-arch while the NOW still formed (Moore et al. 2023), as well as observational studies (Kirillov et al. 2022) and climate simulations (Fol et al. 2025), suggest that the ice-arch will exist less frequently or potentially not at all in the future. In fact, when simulated historical ice area transports through the northern Nares Strait are compared to more recent years when the ice arch was less stable (Moore et al. 2021), the seasonal cycles show somewhat better consistency in terms of magnitude, with key differences remaining in phase (Fig. 6b). For example, in May 2018 and May 2019, when the ice arch was not present, the resultant observed ice area fluxes agree with the simulated May historical climatology, but then decreased in the summer and increased in the fall to levels outside the range of simulated climatology. While it is difficult to draw strong conclusions from comparisons between a 30 year climate model ensemble and four years of observations, this stronger agreement of the CESM1 ice fluxes with more recent observations suggests that simulated ice area fluxes are not unrealistically large in the absence of a stable ice arch. Thus, future Nares Strait sea ice fluxes are likely to exhibit stronger agreement with simulated ice transports in a warmer climate.

Another source of spatial differences in the regions of open water in the post-polynya stage is likely biases in the simulated atmospheric circulation. In the CESM1-LE, the 10-meter wind field climatology over the historical period (Fig. 7) shows a similar circulation pattern and seasonal cycle to ERA-5 winds, with the strongest northerly winds in the winter and spring and the weakest in the summer. However, there are some key differences, such as an approximately 2 m/s wind speed bias in the western NOW south of Nares Strait as well as a wind speed maximum located within the Nares Strait as opposed to south of the strait in ERA-5. Importantly, it has been shown that to resolve all details of the effect of atmospheric forcing on the sea ice - ocean interface in the NOW region, model resolutions below 10 km are needed (Moore and Våge 2018; Gutjahr and Heinemann 2018; Moore 2021; Moore and Imrit 2022; Kohnemann and Heinemann 2025). As a result, the approximately 66 km atmosphere (50 km ocean-sea ice) resolution for CESM1, and 17 km for ERA-5, are both too coarse to capture extreme wind events due to ageostrophic intensification from along-strait pressure gradients and steep topography of the Nares Strait, which play a key role in modulating turbulent surface fluxes in the NOW region (Moore 2021; Gutjahr and Heinemann 2018; Barber et al. 2001a). Note that the CESM1 resolution is the standard resolution of current state-of-the-art climate models, so coupled global model simulations at the required less than 10 km resolution are currently not available. In sum, these biases suggest that in CESM1, the influence of oceanic oceanic sensible heat processes are likely overestimated, while turbulent heat fluxes and ice advection play a lesser role due to biases in ice area fluxes and winds. Nonetheless, despite the challenges described above, the agreement with the observed seasonal cycle of polynya area and ice production lends confidence to use the CESM1 to provide an estimate of the expected large scale oceanographic changes that may occur within the NOW region over the 21st century, in particular for June and July (which show stronger agreement with observations), based on the currently available global, fully-coupled, large ensemble climate simulations.

b. Projected future changes in North Water Polynya ice production and area

As atmospheric warming increases, the polynya has a larger area during the spring due to both reduced sea ice growth and import through Nares Strait during the cold season, helping to precondition a thinner ice cover for an earlier and more expansive spring and summer melt. Decreases in NOW ice production are most pronounced in October and November (Fig. 3),

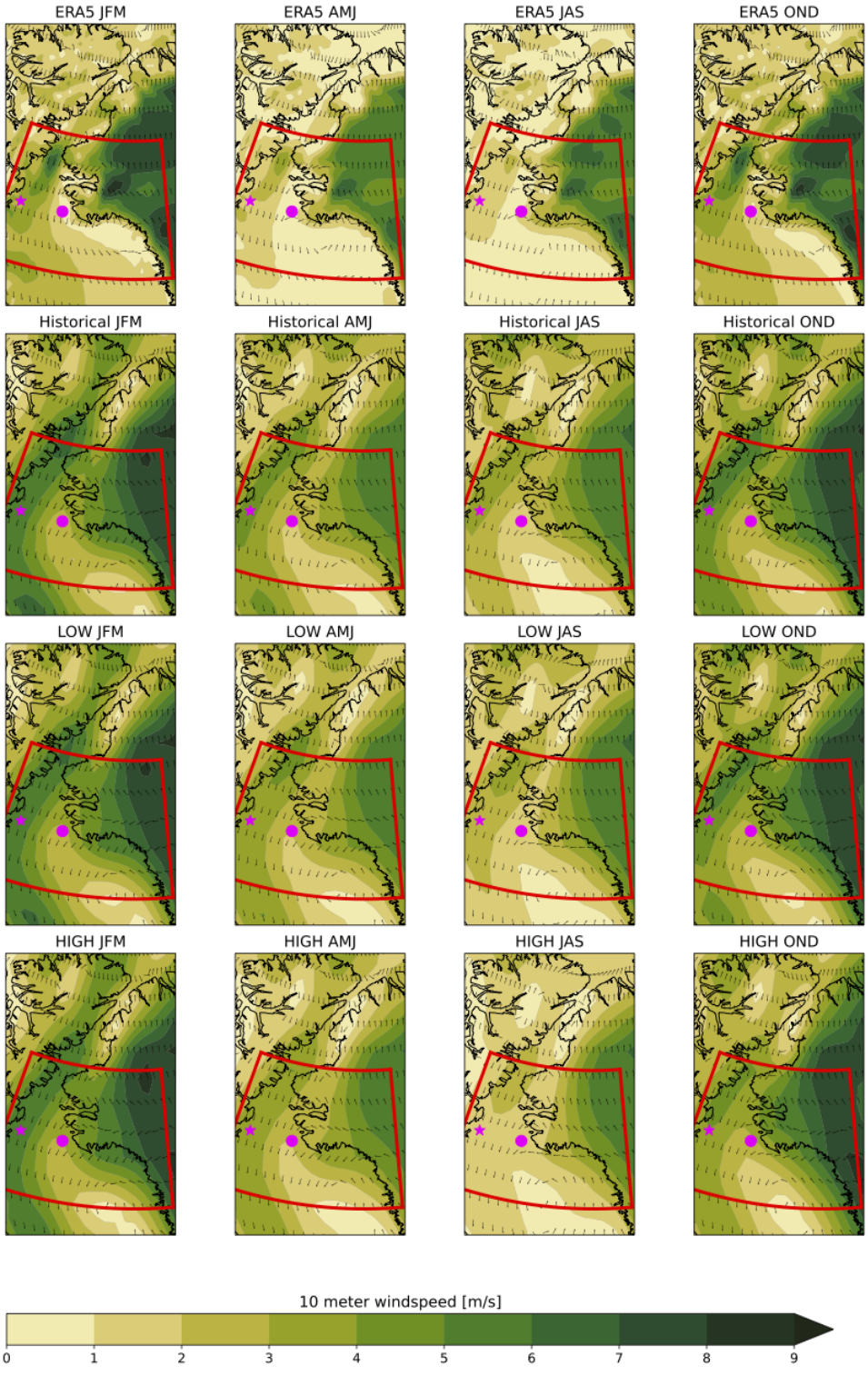

FIG. 7: Spatial map of the 10 meter atmospheric circulation during winter (JFM), spring (AMJ), summer (JAS), and fall (OND) over the NOW region in ERA5 over the historical period (1980-2009), and CESM1 over the historical period, LOW, and HIGH. The extent of the NOW region is shown in red, and the location of ocean section and East and West locations are shown in magenta.

in agreement with recent observational studies in Baffin Bay and modeling studies of Antarctic polynyas, which attribute these changes to surface ocean warming from advected ocean heat transports and enhanced ice-albedo feedback (Ballinger et al. 2022; Jeong et al. 2023a). Under LOW, fall ice growth progresses more slowly and peaks a month later than under historical conditions, but still matches December historical conditions at its peak. Under HIGH however, the entire sea ice growth season is shortened by a month, and the December peak growth is ~ 7 km^3 lower than the November historical peak, driven by minimal ice growth in the southern NOW region (Fig. 5). There are minimal warming level differences in regionally averaged ice growth rates in the winter and spring months, as sea ice thickens in the winter, reducing conductive heat fluxes through the ice, and air temperatures begin to warm in the spring (Fig. 3 & S2). Changes to ice growth with warming level are also accompanied by decreases to solid freshwater import from Nares Strait into the NOW region and reduced solid freshwater export from the southern NOW region into central Baffin Bay (Fig. 6c-d). These changes to winter ice growth, and sea ice import and export, act to thin the winter sea ice cover and accelerate spring sea ice melt and the opening of the polynya. In April, the ensemble mean polynya areas are over 2-3 times larger for LOW and 5 times larger for HIGH compared to the historical period (Fig. 3). For example, in April with a threshold of 5000 km^2, the probability of open waters within the NOW having a total area smaller than this value is 100% for historical conditions but only 98% for LOW and 91% for HIGH (Fig.4). Thus, in the context of internal variability, the likelihood of spring open water areas enlarging increases. In May, a similar pattern occurs, with increases in both average and anomalous polynya areas with warming (Fig. 3 & Fig. 4).

In summer, the NOW area increases with warming when it exists as a polynya. Specifically, in June, the ensemble mean polynya areas are largest for LOW and decrease below historical levels for HIGH (Fig. 3). This is because in more than 40% of June cases for HIGH, the open water in the NOW region is connected to open water in southern Baffin Bay and as a result, the polynya is not considered to be present (see Fig. 4 and Fig. S1). However, when the polynya is present for HIGH in June, the polynya area is larger compared to lower warming scenarios due to more extensive spring melt (Fig. 4). In July, the probability of the polynya entirely disappearing because it connects to open waters in Southern Baffin Bay increases with higher future climate warming. For an open water threshold of 0 km^2 (i.e. no polynya), the cumulative probability of this occurring

is only 80% for historical conditions, but it is 99% for LOW and 100% for HIGH (Fig. 4). In summary, global temperature increases are associated with more extensive sea ice melt and larger polynya areas in the spring, as well as an increased likelihood of polynya disappearance in June and July.

c. Projected future changes in oceanographic conditions

Increasing open water and polynya areas in the NOW region are accompanied by increased stratification in the surface ocean due to warming and freshening. Across the NOW ocean section (see Fig. 2 for its location) in May, waters remain at the freezing point for LOW and see slight warming in the western section for HIGH (Fig. 8). Surface salinities across the section are approximately 2.5 g/kg fresher at HIGH than historically, and 1.5 g/kg fresher compared to LOW (Fig. 9). These differences in surface salinity for different warming levels persist throughout the melt season. For surface temperatures, warming level differences do not emerge until later in the summer in July and August, when increases in surface temperatures compared to the historical period can range from 4-6 °C for HIGH. The effect of these salinity and temperature changes can be seen in the earlier emergence and deepening of the 25.0 σ_θ isopycnal (solid line; Fig. 8 & 9). In the historical period, waters this light are not present in the NOW region until August, and then only in the uppermost 15 meters. As warming increases, this layer of water appears earlier in the summer and deepens: for LOW the 25.0 isopycnal arrives in July at 24 meters depth, and for HIGH this isopycnal is already present in May down to 46 meters and deepens to 80 meters depth by August. Changes in stratification can also be viewed in terms of buoyancy content (Section 2.3), with summer and fall buoyancy increasing with warming levels over the upper 55 meters in the west, east, and total NOW region (Fig. 10a-c). For LOW, upper ocean buoyancy content is driven almost entirely by vertical salinity gradients ($B \approx B_S$), whereas for HIGH, increased stratification is driven by both by both vertical temperature and salinity gradients ($B \approx B_S + B_T$), highlighting the role of upper ocean warming on stratification throughout the NOW region.

Substantial changes are also seen in oceanographic conditions at depth between historical and future periods, namely the warming and salinification of waters below the 27.0 σ_θ isopycnal (dashed line; Fig. 8 & 9). This isopycnal is strongly sloped across the NOW region due to northerly winds and offshore Ekman transport along the west Greenland coast (Melling et al. 2001; Burgers et al.

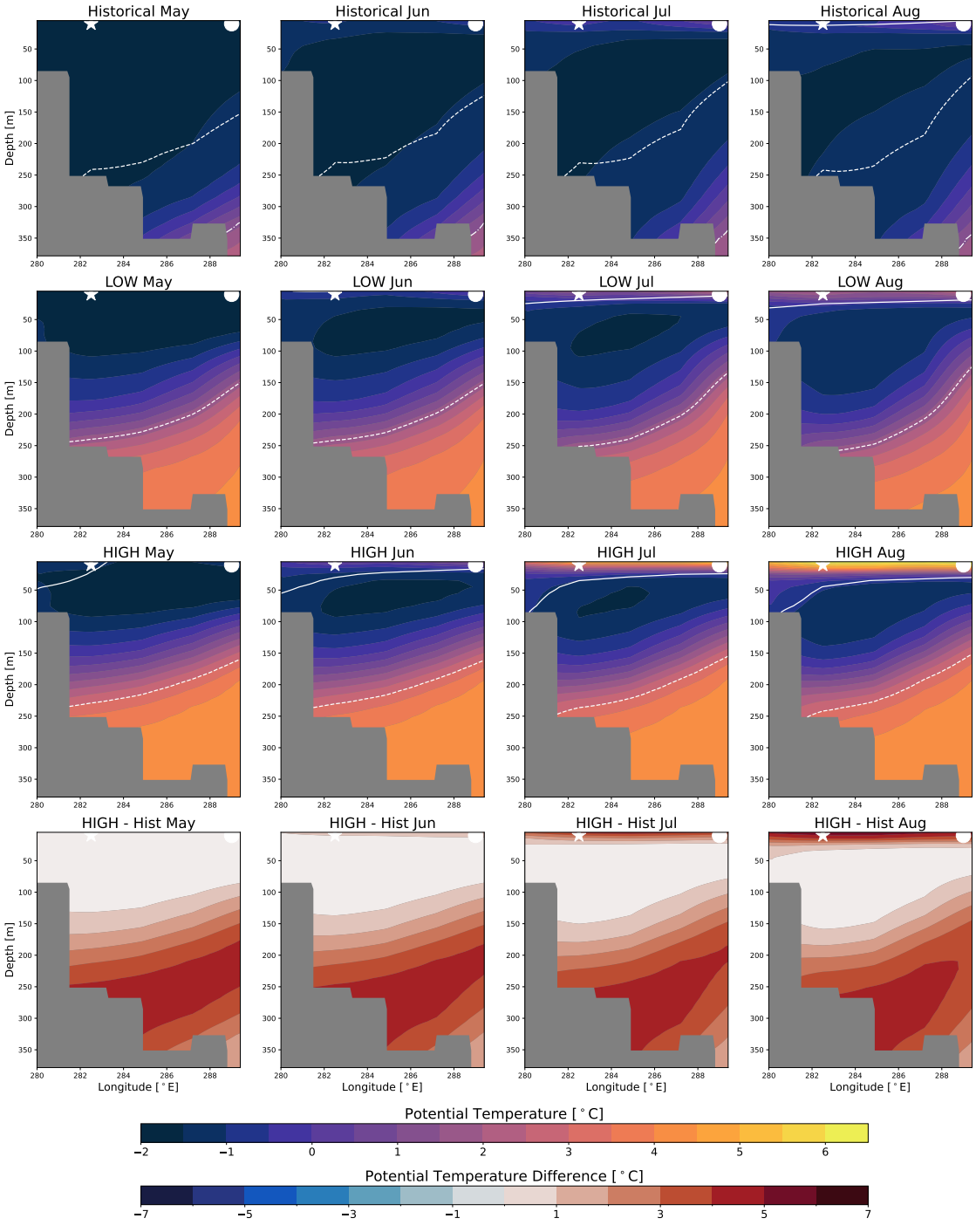

FIG. 8: Cross section of potential temperature along 76.2 °N across the NOW region (see Fig. 2 or 11 for the location of the section) for May through August for the historical period, LOW, and HIGH. The 25.0, 27.0, and 27.5 σ_θ isopycnals are shown in solid, dashed, and dashed-dotted white lines respectively. The bottom row shows the difference between HIGH and historical period. The location of the east and west points used for NPP assessment in Fig. 12 are shown as a white star and circle respectively.

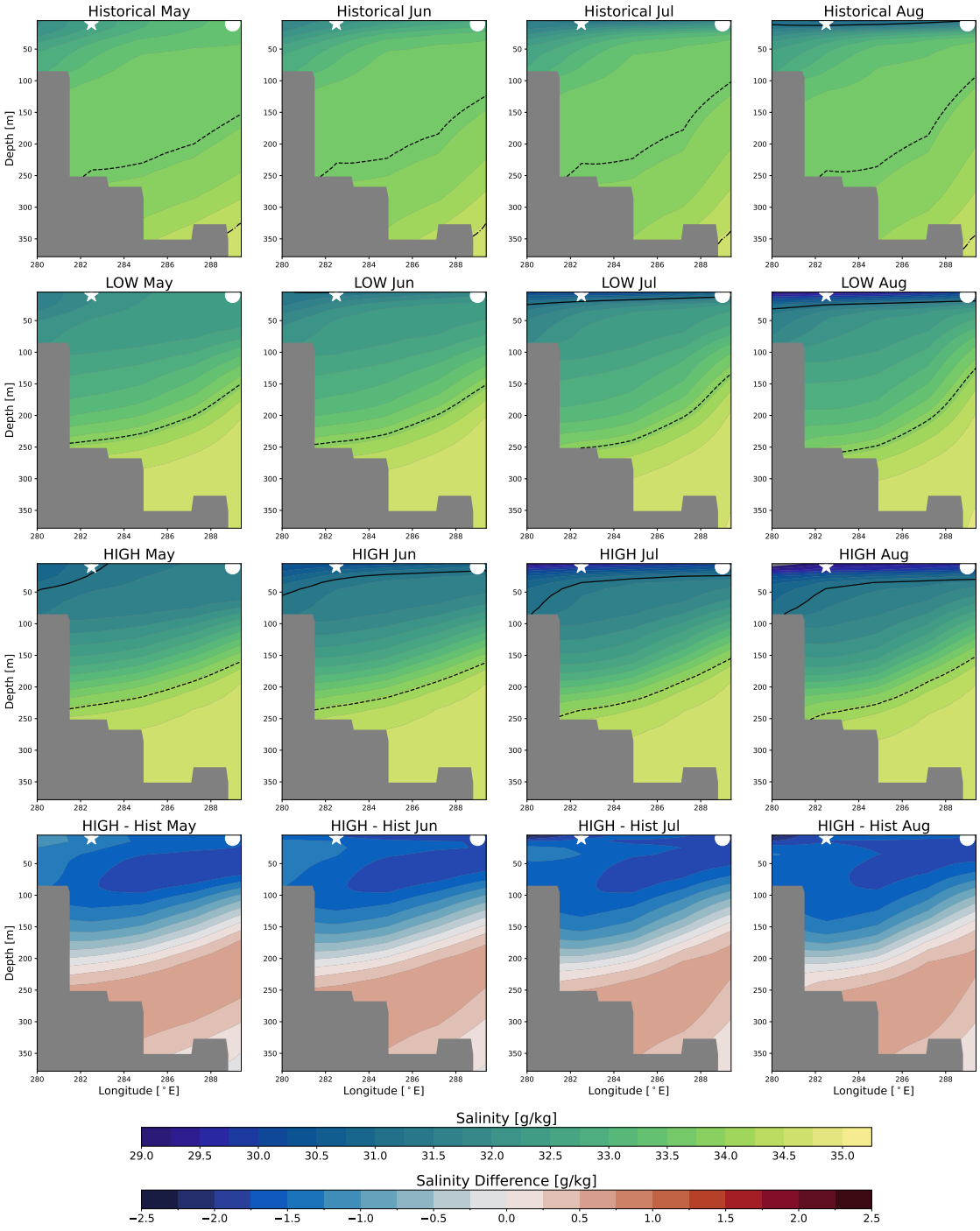

FIG. 9: Cross section of salinity along 76.2 °N across the NOW region (see Fig. 2 or 11 for the location of the section) for May through August historical period, LOW, and HIGH. The 25.0, 27.0, and 27.5 σ_θ isopycnals are shown in solid, dashed, and dash-dotted black lines respectively. The bottom row shows the difference between HIGH and historical period. The location of the east and west points used for NPP assessment in Fig. 12 are shown as a white star and circle respectively.

2023). In the NOW region during the historical period, temperatures and salinities are relatively constant between 50 and 200 meters before increasing with depth. Additionally, in all months of the historical period, cold, salty, waters denser than 1027.5 kg/m^3 are present in at depth in the eastern section in all months (dashed-dotted line; Fig. 8 & 9). The presence of these deep saline waters is in agreement with hydrographic surveys which suggest that while warm, saline WGIW may travel northward into the NOW region before recirculating southwards, WGIW is largely limited to the southern margins of the NOW and can lose much of its heat in transit to the NOW (Melling et al. 2001; Münchow et al. 2015). For all warming levels, however, an increase in temperature and salinity is observed, particularly below 27.0 σ_θ isopycnal, associated with the shoaling and northward penetration of warm WGIWs into the NOW region, as well as the disappearance of waters denser than 1027.5 kg/m^3. This watermass redistribution at depth, contributes to increased stratification throughout the NOW region (Fig. 10d-f) over the upper 155 meters, the approximate depth of the 27.0 σ_θ isopycnal in the eastern NOW, by increasing vertical salinity gradients, despite warmer temperatures at depth partially counteracting the stratification in some regions ($B_S > B$). Increased WGIW at depth is likely due to both increased transports of WGIW into Baffin Bay via the Davis Strait (Castro de la Guardia et al. 2015), as well as an increased transport of WGIW from northern Baffin Bay into the NOW region. An enhanced northward penetration of WGIW into the NOW region is supported by paleoclimate proxies from a warmer climate with a less stable ice arch, increased stratification and reduced brine formation, decreasing densities at depth (Jackson et al. 2021). Importantly, the depth of the 27.0 σ_θ isopycnal does not substantially change with warming, due to the replacement of cold, fresh waters by warmer, saline waters, rendering the mid-depth vertical density structure largely unchanged, and keeping WGIW at a consistent depth in the water column.

d. Future projections of biological conditions

Despite stratification increasing in-step with increasing warming, NPP responds non-linearly and non-uniformly in the NOW region. For historical and all projections, primary production begins in April and May within areas of enhanced sea ice melt on the eastern and western coastal regions of the NOW (Fig. 11 & 12a-c), where exposure of the surface mixed layer to increasing seasonal levels of sunlight leads to a bloom that lasts until August, when the phytoplankton production

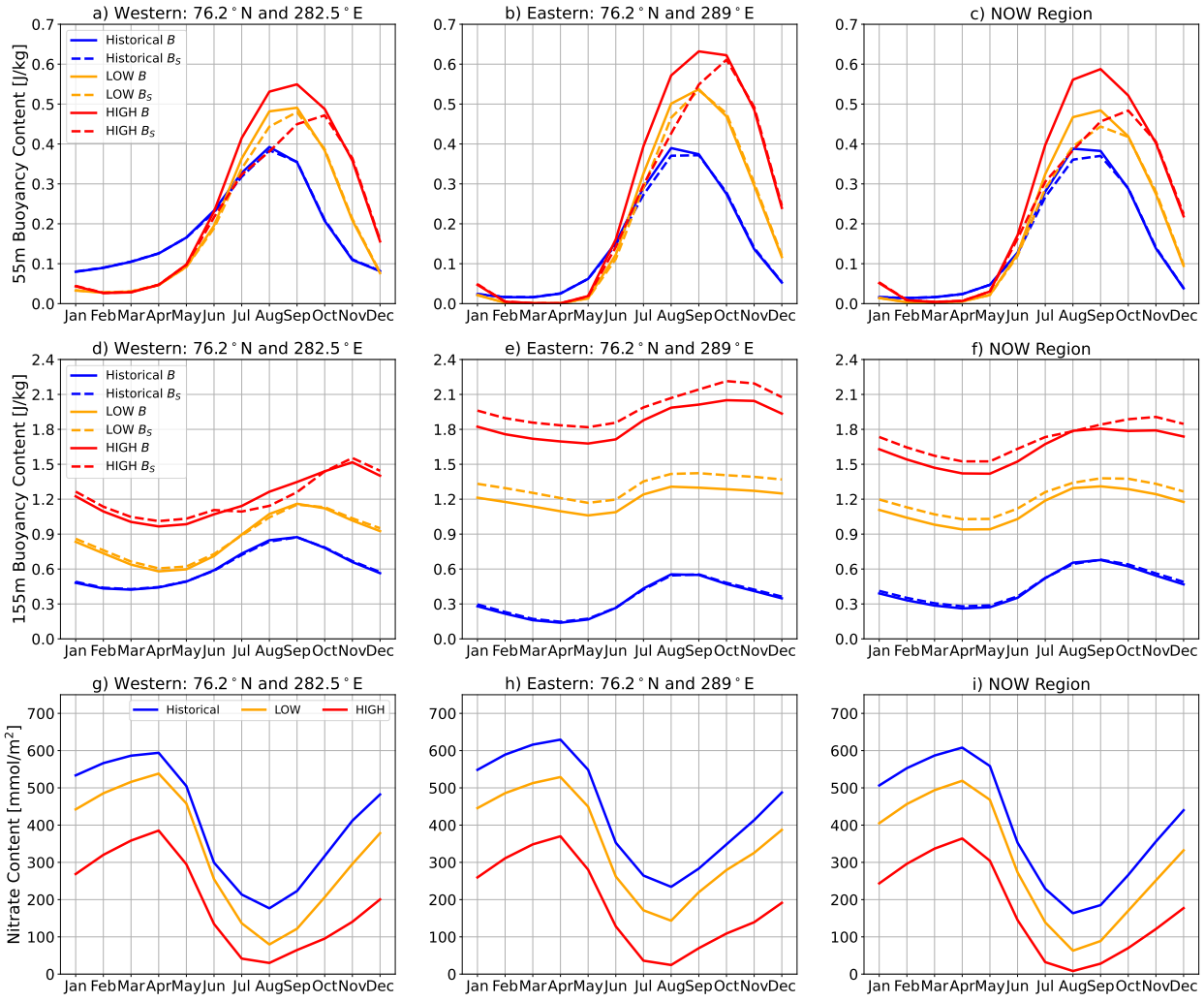

FIG. 10: Buoyancy content for upper 55 meters for a) western, b) eastern, c) NOW region and upper 155 meters for d) western, e) eastern, f) NOW region. Dashed lines show contributions of salinity to buoyancy (B_S) and solid lines show contributions of both temperature and salinity (B). Vertically integrated nitrate content g) western, h) eastern, f) NOW region over upper 55 meters.

has depleted nutrient availability, which coincides with the seasonal decline in sunlight. (Fig. 10g-i; Marchese et al. 2017). For LOW, peak NPP remains similar to historical conditions in the western NOW, but with a shift in the timing of the peak from June to July, whereas in the eastern NOW, July NPP increases by ~12% compared to the historical period. For LOW, peak NPP remains similar to or is greater than historical levels due to the balance between warmer surface temperatures which can increase phytoplankton growth rates, and a more stratified and nutrient depleted upper ocean which limits productivity (Moore et al. 2013; Popova et al. 2012; Vancoppenolle et al. 2013; Wolf et al. 2024; Marinov et al. 2010). The increase in peak NPP in

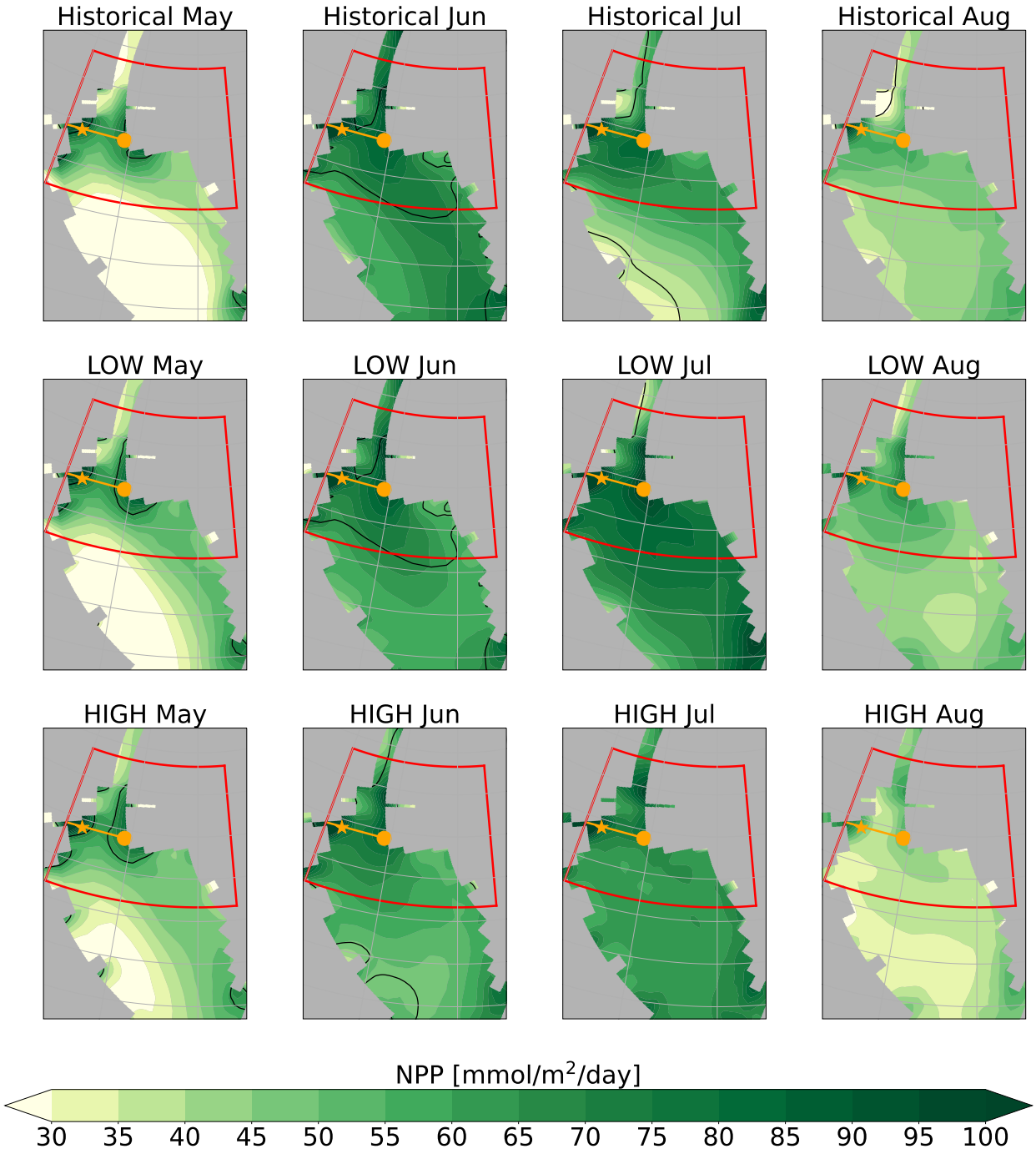

FIG. 11: Spatial map of ensemble mean net primary productivity (NPP) for May through August for the historical period, LOW, and HIGH. The NOW section is shown in orange, with the position of the eastern location marked with a orange dot and the position for the western location marked with a orange star. Black line shows the 70% SIC contour. The red box shows the NOW region.

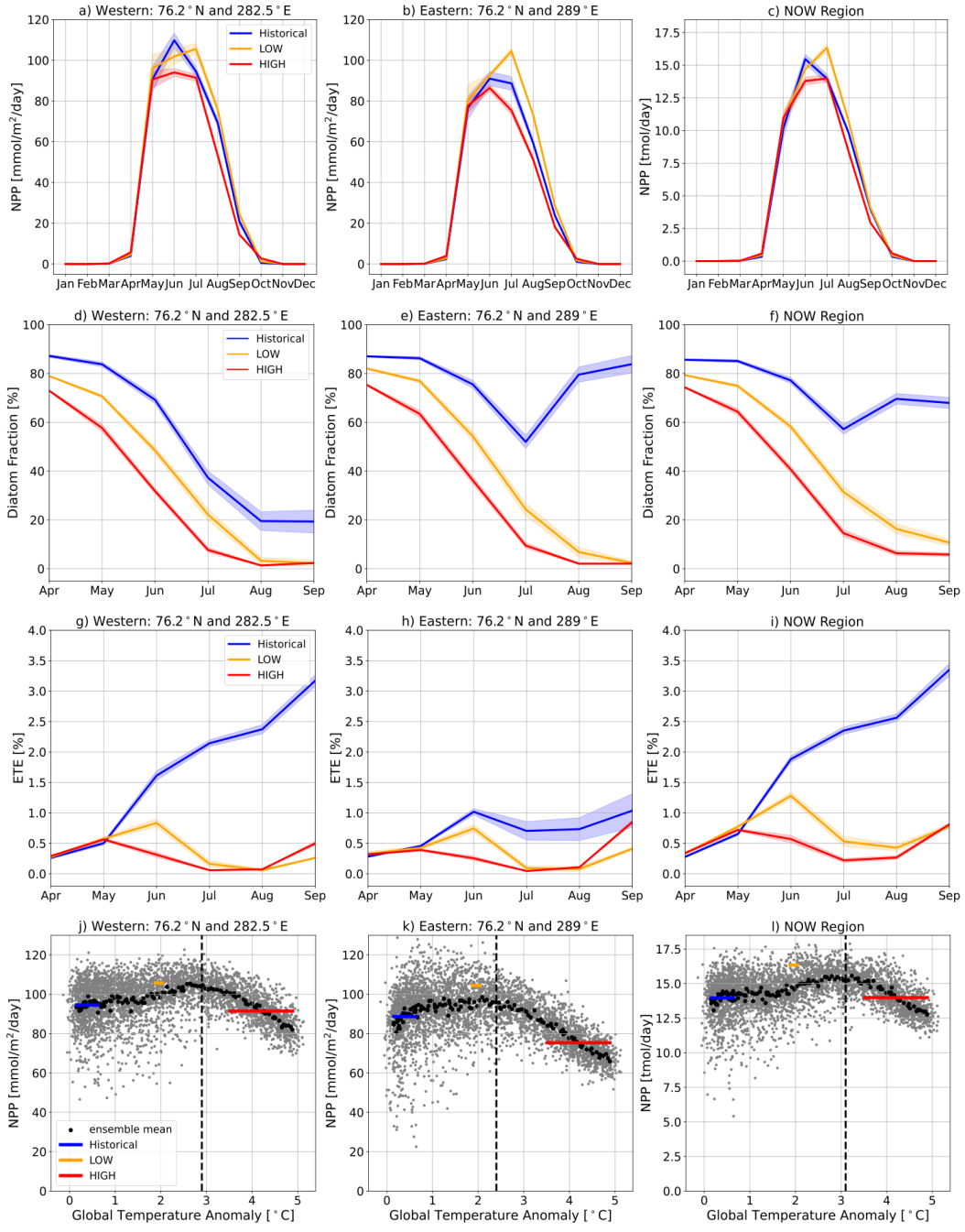

FIG. 12: Seasonal cycle of ensemble mean (a-c) net primary productivity (NPP), (d-f) diatom fraction, and (g-i) Ecosystem Transfer efficiency (ETE) for the historical period, LOW, and HIGH at the a,d,g,j) western location, b,e,h,k) eastern location, and c,f,i,l) total NOW region (see Fig 11 for precise positions). Shading indicates ±1 standard deviation of seasonal cycles between ensemble members, for panels a–i). Note that x-axes only show April through September for d–i (second and third row). The bottom row (j-l) shows the July NPP vs warming level for the entire CESM1-LE simulation from 1980-2100 at the j) western location, h) eastern location, and l) total NOW region. Ensemble mean NPP values are shown in black and individual ensemble members are shown in grey. Average July NPP values based on the 30yr ensemble mean historical period, LOW, and HIGH are shown in blue, orange, and red respectively. The vertical dotted black line shows the transition point when NPP begins to decline based on segmented linear regression analysis.

the eastern NOW relative to the western NOW can be attributed to the ocean circulation of Baffin Bay. The western NOW is directly downstream of the cold polar surface water outflow from the Nares Strait, keeping ocean temperatures cooler and limiting a temperature driven increase in NPP. This is in contrast to the eastern NOW, which receives slightly warmer surface waters traveling northward from central Baffin Bay. For HIGH, peak NPP declines by 14% and 15% in the west and east respectively compared to the historical period (Fig. 12a-b). For HIGH, the surface ocean is too strongly stratified and nutrient limited for warmer waters to increase productivity, leading to a pronounced decrease in peak productivity in both regions despite warm surface temperatures and available nutrients at depth (Fig. 8 & S3). When integrated over the entire NOW region (Fig. 12c), the seasonal cycles of productivity show a shift in peak productivity from June to July with increasing warming levels, a slight increase in peak productivity for LOW, and a decrease in peak productivity for HIGH. There is also a decline in annually integrated productivity by ~5% compared to historical levels for HIGH, substantially less than the declines in annual productivity of 10% and 8% in the west and east, respectively, for the same warming level. This regional difference is due to the partial compensation of the decline in the highest productivity regions in the east and the west of the NOW under HIGH by a small increase in productivity in the Nares Strait due to declining SIC, resulting in warmer temperatures and increased exposure of the surface mixed layer to sunlight (Fig. 11).

Changes in NPP are accompanied by changes in phytoplankton community composition. In the historical period during the early summer, diatoms are the dominant phytoplankton type across all regions, as seen in the diatom fractions (see Section 3e; Fig. 12d-f). In the western NOW, diatom fractions decline throughout the growth season as the surface ocean becomes more nutrient limited. While both small phytoplankton and diatoms are primarily limited by nitrogen in the spring and summer, small phytoplankton out-compete diatoms in nitrogen poor environments leading to a decrease in diatom fraction as the growth season progresses (Moore et al. 2013). In the eastern and total NOW region however, diatom fraction remains above 50% year round, reaching its annual minimum in July, before increasing in August and September (Fig. 12e-f). The year round dominance of diatoms in the eastern and greater NOW region during the historical period highlights both the role of coastal upwelling in the eastern NOW, resupplying the surface ocean with nutrients, as well as the reduced light limitation of diatoms, which allow diatoms to out-compete

small phytoplankton in nutrient-rich, light poor environments (Krumhardt et al. 2022; Moore et al. 2013; Marinov et al. 2010). Across all regions and months, diatoms become less dominant with increased warming compared to small phytoplankton, and exhibit a spatially uniform seasonal cycle resembling the western NOW in the historical period, with high diatom fraction in spring but declining to ~15% or less by September (Fig. 12d-f). In warmer climates in the eastern NOW, the lack of diatom resurgence in the late summer is notable, and strongly suggests that even for LOW, stratification is too strong to bring the abundant nutrients at depth to the surface.

Reductions in diatom fractions have large implications for the NOW ecosystem, reducing the energy available for consumption at higher trophic levels. ETE (Estimated Trophic Efficiency; see Section 2e) is reduced compared to historical conditions in May through September, especially in the western and total NOW regions (Fig. 12g-i). High ETE in the late summer during the historical period is due to the seasonal cycle of mesozooplankton production lagging behind the NPP seasonal cycle in the historical period, peaking in July as opposed to June and increasing the ratio of mesozooplankton production to NPP (Fig. S4). In the eastern NOW, historical ETE is smaller than the west due to reduced mesozooplankton production, and NPP and mesozooplankton production both peaking concurrently in June. In all warming scenarios, mesozooplankton production is substantially reduced, which combined with declining diatom fractions, leads to over 50% reductions in ETE during most months relative to historical conditions. Critically, mesozooplankton production and ETE declines in June for LOW in the eastern NOW despite increases in NPP compared to the historical period (Fig. 12h & S4b), highlighting that, at higher trophic levels, the impacts of changing phytoplankton community composition outweigh increased primary production. Note that, the total and eastern NPP seasonal cycles for LOW, all HIGH NPP seasonal cycles, as well as diatom fraction and ETE for all warming levels, exhibit changes outside the ensemble spread of historical seasonal cycles (Fig. 12a-i). As a result, we can conclude that changes between the different ocean states underlying these productivity regimes are driven by external forcing (warming level), as opposed to internal climate variability. In summary, while end of 21st century peak NPP will remain constant or increase if warming remains below 2 °C, changes in community composition will substantially reduce the trophic efficiency of the NOW ecosystem, with likely negative impacts to the NOW ecosystem and the people who rely on it (Stock et al. 2017; Grønnow 2016).

4. Discussion

We find that profound changes in biological productivity in the NOW in a warming climate are associated with reduced cold season ice growth, reduced sea ice import and export, larger spring open water areas and earlier polynya disappearances, and are driven by the balance between increases in temperatures, increased stratification, and decreased nutrient availability in the upper ocean. For both investigated warming levels, surface freshening in the NOW region is driven by a combination of changes in sea ice melt, runoff, and Arctic Ocean freshwater export through Nares Strait. Previous work with the CESM1 (Jahn and Laiho 2020), and other climate models (Rasmussen et al. 2011; Zanowski et al. 2021), have shown that Nares Strait liquid freshwater fluxes are projected to increase and solid fluxes are predicted to decrease with climate warming, supporting the increases in stratification seen at LOW and HIGH. Despite biases in Nares Strait ice area fluxes during the historical period, the agreement between CESM1 and more recent ice area flux observations (Moore et al. 2021) lends confidence to our future projections of solid freshwater import into the NOW, as well as its downstream impacts on stratification in the NOW and freshwater transports to southern Baffin Bay (Fig. 6). While CESM1 does not include a coupled ice-sheet model, simulated runoff also increases with warming level (Fig. S5), and, along with freshwater from the Nares Strait and local sea ice melt, provides an additional source of freshwater to promote increased stratification, in agreement with other modeling studies that explicitly prescribe glacial discharge (Buchart et al. 2022). However, the influence of glacial meltwater on biological conditions in the NOW is a source of uncertainty. It is possible that the additional glacial freshwater input could reinforce stratification and further reduce nutrient transport to the surface mixed layer (Buchart et al. 2022); Or, freshwater plumes from basal melt could entrain nutrients and provide a mechanism for nutrient delivery to the surface despite increased stratification (Kanna et al. 2018). Furthermore, given the uncertainties associated with both ice area fluxes and glacial meltwater, a sensitivity study using a high-resolution fully coupled, ocean–sea ice–ice sheet model, with updated sea ice stress and landfast ice parameterizations (Lemieux et al. 2016; Sterlin et al. 2024), should be carried out to assess these questions in the future. In short, despite the uncertainty related to Baffin Bay freshwater inputs, this study highlights the key roles that both long-range Arctic freshwater export and local runoff and sea ice melt plays in modulating physical and biological oceanographic conditions in the NOW region.

NPP changes in the NOW region with warming are driven by the delicate balance between increasing stratification, which decreases surface nutrient content, and increasing water temperatures, which increase phytoplankton growth rates. In all regions of the NOW, July NPP increases with warming until a certain increase in global mean temperature, after which productivity begins to decline as decreased nutrient availability limits NPP (Fig. 12j-l), exhibiting the inverted-U phenomenon, which is present in many marine ecosystems undergoing environmental change (e.g. Eppley 1972; Ballerini et al. 2015). While NPP decreases for HIGH in the NOW region, other studies (Vancoppenolle et al. 2013; Noh et al. 2023) have found an increase in Arctic Ocean NPP for higher levels of warming (HIGH equivalent). In the Arctic Ocean, modest NPP increases are due to the balance between sea ice decline, driving warmer temperatures and increased light availability, and decreased nutrients in surface waters (Vancoppenolle et al. 2013). The diverging projections for the NOW and the Arctic Ocean NPP for HIGH are due to 1) greater production in the NOW region during the historical period compared to the Arctic due to greater nutrient and light availability (Marchese et al. 2017), and 2) the reduced importance of changing light limitation in the NOW region. As an active polynya, sea ice opens earlier in the spring compared to the central Arctic Ocean (Fig. 2), allowing the growth season to begin earlier. As a result, in the NOW, light limitation is primarily due to seasonal cycle of solar insolation instead of the presence of sea ice, as can be seen in the lack of April NPP change between the historical period, LOW, and HIGH (Fig. 12a-c). Therefore, declining sea ice concentrations in the Arctic Ocean have a greater influence on reducing light limitations compared to the NOW (Vancoppenolle et al. 2013). This leads to diverging projections of NPP between the NOW region and Arctic Ocean for HIGH. In sum, these findings imply the NPP in the Arctic Ocean may become more spatially uniform for HIGH, as NPP is projected to decrease in the NOW region and increase in the Arctic Ocean (Vancoppenolle et al. 2013; Noh et al. 2023).

An analysis using segmented linear regressions across the CESM1-LE from 1980 to 2100 shows that the transition between increasing NPP, when ocean warming increases phytoplankton growth, and decreasing NPP, when nutrients become too limited to support increased growth, occurs at approximately 2.9, 2.4, and 3.1 °C for the western, eastern, and total NOW regions, respectively (Fig. 12j-l). The warmer transition point in the total NOW region, compared to the east and west, is in agreement with Buchart et al. (2022) who found that regionally averaged NPP in the NOW

only weakly responded to climate warming. The higher regional versus local sensitivity to climate warming also adds to a body of work highlighting the importance of sub-regional spatial scales in the NOW region (Bailey et al. 2013). Even in the presence of spatial SIC biases due to coarse model resolution and weak internal ice stress, we have confidence in these sub-regional differences in biological productivity, as they are based on the underlying simulated ocean circulation and watermass distributions, which are supported by both historical observations (Tang et al. 2004; Burgers et al. 2023) and paleoclimate proxies (Jackson et al. 2021). That said, due to model biases the exact temperature thresholds associated with these biological changes are a source of uncertainty. Notably, productivity is higher in the LOW simulations that are at a steady warming level compared to the ensemble mean NPP from the transient CESM1-LE forced by RCP8.5 at the same warming level (Fig. 12g-i). These differences suggest that the NOW will respond differently to a short-lived climatic state when warming is continuously increasing (transient) versus when a global temperature anomaly is constant. The reduced forced response and high internal variability of biological productivity when continuous climate warming is below present day warming of $<1.5^{\circ}$C (Fig. 12j-l) helps to contextualize observed changes in the NOW region, and indicates that observed declines in peak phytoplankton bloom amplitudes in the NOW region are most likely due to internal variability and not climate warming (Marchese et al. 2017). Furthermore, the NPP response for transient vs constant temperature anomalies can further help explain why this study sees a stronger response in NPP to climatic warming compared to Buchart et al. (2022), who used transient (RCP 4.5 & 8.5) greenhouse gas forcings.

In the NOW region, higher NPP does not correspond to increased productivity at higher trophic levels (Deb and Bailey 2023). The NOW owes its large ecosystem productivity to upwelling in the eastern NOW, which supports a large diatom population during the historical period. Even under LOW, however, coastal upwelling is sufficiently limited by stratification and is unable to provide a meaningful source of nutrients to the surface mixed layer, despite increasing nutrient concentrations at depth (Fig. 10g-i & S3). Increased production of small phytoplankton in response to warmer ocean temperatures and more limited nutrients is not able to make up for the loss of diatom production, leading to a decline in ETE and productivity at higher trophic levels, even in the context of increasing NPP in some regions (Fig. 12g-i & S4). As a result, model representation of phytoplankton community composition and atmospheric circulation, in

the context of coastal upwelling providing a sufficient nutrient sources for diatoms, plays a crucial role in projections of ecosystem productivity at higher trophic levels. For example, phytoplankton community composition is highly simplified in CESM1, only including two phytoplankton types that are not Arctic specific (Moore et al. 2013), as in most CMIP5 an CMIP6 models (Popova et al. 2012; Séférian et al. 2020). In addition, productivity at higher trophic levels neglects benthic ecosystems and is not simulated directly in the model (Krumhardt et al. 2022). As a result, the simulations presented almost certainly neglect key biological processes that influence NPP, diatom populations, and their energy transfer to higher trophic levels. Furthermore, projections of reduced production at higher trophic levels with climate warming is dependent on whether wind-induced upwelling is strong enough to overcome the stratification and resupply the mixed layer with increasing nutrients at depth. Importantly, northerly winds in the NOW region remain at a consistent magnitude under both LOW and HIGH, suggesting that potential changes to the regional atmospheric circulation, and its influence on upwelling in the eastern NOW, cannot explain the projected physical and biological ocean changes with warming (Fig. 7). Although projections of the atmospheric circulation and air-sea interactions are a source of uncertainty due to the coarse model resolution (Moore and Våge 2018; Gutjahr and Heinemann 2018; Jeong et al. 2023b), our findings of minimal changes to atmospheric circulation are in agreement with other modeling studies which found negligible changes to wind stress in northern Baffin Bay (Muilwijk et al. 2024), lending confidence to our projections of reduced upwelling, reduced nutrient availability, and reduced ecosystem productivity at higher trophic levels in the NOW region.

In summary, dedicated, policy relevant, low-warming climate simulations demonstrate that under less than 2 °C warming globally, while NPP is expected to be similar to or higher than during historical conditions, shifts in phytoplankton community composition that impact higher trophic levels should be expected. Critically, even in CESM1 simulations when global warming is limited to 1.5 °C (Sanderson et al. 2017), an increasingly unlikely emissions scenario (Gulev et al. 2021), diatom fraction still declines in similar manner to LOW (not shown), implying a reduction in higher trophic level productivity even under modest warming. Therefore, regardless of the future emission scenario, the NOW region will likely see reductions in ecosystem productivity, with impacts to Greenlandic and Inuit communities.

5. Conclusions

The North Water Polynya (NOW) is one of the most productive biological regions in the Arctic with high importance to local and Inuit and Greenlandic comunities (Hastrup et al. 2018; Ribeiro et al. 2021). To provide insights into the potential changes of this region as global temperatures rise, we investigated the physical and biological oceanic responses of the NOW region to <2 °C (LOW) and >3.5 °C (HIGH) warming using the CESM1 climate model (Sanderson et al. 2017; Kay et al. 2015; Hurrell et al. 2013). We showed that global temperature increases are associated with reduced winter sea ice production, reduced sea ice import and export, accelerated spring sea ice melt, and larger open water areas that are no longer distinct from central Baffin Bay open waters. For both LOW and HIGH, increased polynya areas and sea ice melt occur alongside increased stratification, isolating surface waters from those at depth, decreasing surface nutrient concentrations, and leading to increased concentrations of nutrient-rich West Greenland Irminger Waters (WGIW) throughout the NOW region. For LOW, warmer water temperatures increase phytoplankton growth rates despite decreased nutrients, resulting in minimal NPP changes in the western NOW region and increasing peak NPP in the eastern NOW. For HIGH however, the influence of increasing stratification and decreased nutrient concentrations with continued climate warming outweighs increased growth rates from warmer water temperatures, leading to a decline in NPP in the eastern and western NOW. We also find that changes to the atmospheric circulation (which drive upwelling) and light limitation plays a minimal role in projected NPP changes in the NOW. Critically, in all regions and scenarios, changes in peak NPP are accompanied by the decreasing presence of diatoms in the NOW region, especially in the late summer, resulting in dramatic reductions in ETE (Energy Transfer Efficiency) and productivity in higher trophic levels, even when global warming is <2 °C (and <1.5 °C). These results, in concert with the small influence of internal climate variability on these processes, point to the importance of limiting global temperature increases to well below <1.5 °C to protect the NOW ecosystem and the communities who depend on it.

Acknowledgments. This study was supported by NSF award 1804504. We also acknowledge NSF CAREER award 1847398, as this manuscript grew out of a project in a Course Based Research experience (CURE) class at CU Boulder taught as part of award 1847398, which also supported the contribution of C. Wyburn-Powell, P. Ugrinow, and R. Patel and the early work on the project by A. Jahn. We would also like to acknowledge high-performance computing on Cheyenne provided by NCAR's Computational and Information Systems Laboratory, sponsored by the National Science Foundation. We thank Thomas Juul-Pedersen for discussions on biogeochemical dynamics in Baffin Bay, Kristen Krumhardt for discussions about NPP in the CESM1, Anna-Marie Strehl for discussions on stratification, and Ivonne Martinez and Patricia DeRepentigny for early exploratory work on the future evolution of the NOW. We thank Stephen Howell, Martin Vancoppenolle, and the other anonymous reviewers for their substantive comments, which greatly improved the final manuscript.

Data availability statement. Model output from the CESM1 can be found at https://ncar.github.io/cesm-lens-aws/ and https://www2.cesm.ucar.edu/experiments/1.5-2.0-targets.html. Observed sea ice concentrations are available at https://nsidc.org/data/g02202/versions/4. Nares Strait ice area fluxes from 2017 and 2018 (Moore et al. 2021) are available from https://borealisdata.ca/dataset.xhtml?persistentId=doi:10.5683/SP2/WRGX0K. ERA5 winds are available at https://cds.climate.copernicus.eu/datasets/reanalysis-era5-single-levels-monthly-means?tab=download.

References

Bailey, J. N. L., R. W. Macdonald, H. Sanei, P. M. Outridge, S. C. Johannessen, K. Hochheim, D. Barber, and G. A. Stern, 2013: Change at the margin of the North Water Polynya, Baffin Bay, inferred from organic matter records in dated sediment cores. *Marine Geology*, **341**, 1–13, https://doi.org/10.1016/j.margeo.2013.04.017.

Ballerini, T., G. Tavecchia, F. Pezzo, S. Jenouvrier, and S. Olmastroni, 2015: Predicting responses of the Adélie penguin population of Edmonson Point to future sea ice changes in the Ross Sea. *Frontiers in Ecology and Evolution*, **3**, https://doi.org/10.3389/fevo.2015.00008.

Ballinger, T. J., G. W. K. Moore, Y. Garcia-Quintana, P. G. Myers, A. A. Imrit, D. Topal, and W. N. Meier, 2022: Abrupt Northern Baffin Bay Autumn Warming and Sea-Ice Loss Since the Turn of the Twenty-First Century. *GEOPHYSICAL RESEARCH LETTERS*, **49 (21)**, e2022GL101 472, https://doi.org/10.1029/2022GL101472.

Barber, D., J. Hanesiak, W. Chan, and J. Piwowar, 2001a: Sea-ice and meteorological conditions in Northern Baffin Bay and the North Water polynya between 1979 and 1996. *Atmosphere-Ocean*, **39 (3)**, 343–359, https://doi.org/10.1080/07055900.2001.9649685.

Barber, D., R. Marsden, P. Minnett, G. Ingram, and L. Fortier, 2001b: Physical processes within the North Water (NOW) polynya. *Atmosphere-Ocean*, **39 (3)**, 163–166, https://doi.org/10.1080/07055900.2001.9649673.

Bi, H., Z. Zhang, Y. Wang, X. Xu, Y. Liang, J. Huang, Y. Liu, and M. Fu, 2019: Baffin Bay sea ice inflow and outflow: 1978–1979 to 2016–2017. *The Cryosphere*, **13 (3)**, 1025–1042, https://doi.org/10.5194/tc-13-1025-2019.

Buchart, L., and Coauthors, 2022: Future Climate Scenarios for Northern Baffin Bay and the Pikialasorsuaq (North Water Polynya) Region. *Atmosphere-Ocean*, **0 (0)**, 1–22, https://doi.org/10.1080/07055900.2022.2067028.

Burgers, T. M., L. A. Miller, S. Rysgaard, J. Mortensen, B. Else, J.-É. Tremblay, and T. Papakyriakou, 2023: Distinguishing Physical and Biological Controls on the Carbon Dynamics in a High-Arctic Outlet Strait. *Journal of Geophysical Research: Oceans*, **128 (3)**, e2022JC019 393, https://doi.org/10.1029/2022JC019393.

Castro de la Guardia, L., X. Hu, and P. G. Myers, 2015: Potential positive feedback between Greenland Ice Sheet melt and Baffin Bay heat content on the west Greenland shelf. *Geophysical Research Letters*, **42 (12)**, 4922–4930, https://doi.org/10.1002/2015GL064626.

Deb, J. C., and S. A. Bailey, 2023: Arctic marine ecosystems face increasing climate stress. *Environmental Reviews*, **31 (3)**, 403–451, https://doi.org/10.1139/er-2022-0101.

DeRepentigny, P., A. Jahn, M. M. Holland, and A. Smith, 2020: Arctic Sea Ice in Two Configurations of the CESM2 During the 20th and 21st Centuries. *Journal of Geophysical Research: Oceans*, **125 (9)**, e2020JC016 133, https://doi.org/10.1029/2020JC016133.

Dumont, D., Y. Gratton, and T. E. Arbetter, 2009: Modeling the Dynamics of the North Water Polynya Ice Bridge. *Journal of Physical Oceanography*, **39 (6)**, 1448–1461, https://doi.org/10.1175/2008JPO3965.1.

Dumont, D., Y. Gratton, and T. E. Arbetter, 2010: Modeling Wind-Driven Circulation and Landfast Ice-Edge Processes during Polynya Events in Northern Baffin Bay. *Journal of Physical Oceanography*, **40 (6)**, 1356–1372, https://doi.org/10.1175/2010JPO4292.1.

Dunbar, M., and M. Dunbar, 1972: The history of the North Water. *Proceedings of the Royal Society of Edinburgh, Section B: Biological Sciences*, **72**, 231–241.

DuVivier, A. K., M. M. Holland, J. E. Kay, S. Tilmes, A. Gettelman, and D. A. Bailey, 2020: Arctic and Antarctic Sea Ice Mean State in the Community Earth System Model Version 2 and the Influence of Atmospheric Chemistry. *Journal of Geophysical Research: Oceans*, **125 (8)**, e2019JC015 934, https://doi.org/10.1029/2019JC015934.

Eppley, R. W., 1972: Temperature and phytoplankton growth in the sea. *Fishery Bulletin*, **70**, 1063–1085.

Fol, M., B. Tremblay, S. Pfirman, R. Newton, S. Howell, and J.-F. Lemieux, 2025: Revisiting the Last Ice Area projections from a high-resolution Global Earth System Model. *Communications Earth & Environment*, **6 (1)**, 1–12, https://doi.org/10.1038/s43247-025-02034-5.

Georgiadis, E., J. Giraudeau, A. Jennings, A. Limoges, R. Jackson, S. Ribeiro, and G. Massé, 2020: Local and regional controls on Holocene sea ice dynamics and oceanography in Nares

Strait, Northwest Greenland. *Marine Geology*, **422**, 106 115, https://doi.org/10.1016/j.margeo.2020.106115.

Gjelstrup, C. V. B., and C. A. Stedmon, 2024: A switch in thermal and haline contributions to stratification in the Greenland Sea during the last four decades. *Progress in Oceanography*, **225**, 103 283, https://doi.org/10.1016/j.pocean.2024.103283.

Grønnow, B., 2016: Living at a High Arctic Polynya: Inughuit Settlement and Subsistence around the North Water during the Thule Station Period, 1910–53. *ARCTIC*, **69 (5)**, 1–15, https://doi.org/10.14430/arctic4573.

Gulev, S. K., and Coauthors, 2021: Changing state of the climate system. *Climate Change 2021: The Physical Science Basis. Contribution of Working Group I to the Sixth Assessment Report of the Intergovernmental Panel on Climate Change*, V. Masson-Delmotte, P. Zhai, A. Pirani, S. L. Connors, C. Péan, S. Berger, N. Caud, Y. Chen, L. Goldfarb, M. I. Gomis, M. Huang, K. Leitzell, E. Lonnoy, J. B. R. Matthews, T. K. Maycock, T. Waterfield, Ö. Yelekçi, R. Yu, and B. Zhou, Eds., Cambridge University Press, Cambridge, United Kingdom and New York, NY, USA, 287–422, https://doi.org/10.1017/9781009157896.001.

Gutjahr, O., and G. Heinemann, 2018: A model-based comparison of extreme winds in the Arctic and around Greenland. *International Journal of Climatology*, **38 (14)**, 5272–5292, https://doi.org/10.1002/joc.5729.

Harning, D. J., B. Holman, L. Woelders, A. E. Jennings, and J. Sepúlveda, 2023: Biomarker characterization of the North Water Polynya, Baffin Bay: implications for local sea ice and temperature proxies. *Biogeosciences*, **20 (1)**, 229–249, https://doi.org/10.5194/bg-20-229-2023.

Hastrup, K., A. Mosbech, and B. Grønnow, 2018: Introducing the North Water: Histories of exploration, ice dynamics, living resources, and human settlement in the Thule Region. *Ambio*, **47 (Suppl 2)**, 162–174, https://doi.org/10.1007/s13280-018-1030-2.

Hausfather, Z., K. Marvel, G. A. Schmidt, J. W. Nielsen-Gammon, and M. Zelinka, 2022: Climate simulations: recognize the 'hot model' problem. *Nature*, **605 (7908)**, 26–29, https://doi.org/10.1038/d41586-022-01192-2.

739 Heide-Jørgensen, M. P., L. M. Burt, R. G. Hansen, N. H. Nielsen, M. Rasmussen, S. Fossette, and
740 H. Stern, 2013: The Significance of the North Water Polynya to Arctic Top Predators. *AMBIO*,
741 **42 (5)**, 596–610, https://doi.org/10.1007/s13280-012-0357-3.

742 Heide-Jørgensen, M. P., M.-H. S. Sinding, N. H. Nielsen, A. Rosing-Asvid, and R. G. Hansen,
743 2016: Large numbers of marine mammals winter in the North Water polynya. *Polar Biology*,
744 **39 (9)**, 1605–1614, https://doi.org/10.1007/s00300-015-1885-7.

745 Howell, S. E. L., D. G. Babb, J. C. Landy, G. W. K. Moore, T. J. Ballinger, K. McNeil, B. Montpetit,
746 and M. Brady, 2024: Baffin Bay Ice Export and Production From Sentinel-1, the RADARSAT
747 Constellation Mission, and CryoSat-2: 2016–2022. *Geophysical Research Letters*, **51 (22)**,
748 e2024GL111 364, https://doi.org/10.1029/2024GL111364.

749 Howell, S. E. L., D. G. Babb, J. C. Landy, G. W. K. Moore, B. Montpetit, and M. Brady,
750 2023: A Comparison of Arctic Ocean Sea Ice Export Between Nares Strait and the Canadian
751 Arctic Archipelago. *Journal of Geophysical Research: Oceans*, **128 (4)**, e2023JC019 687,
752 https://doi.org/10.1029/2023JC019687.

753 Hurrell, J. W., and Coauthors, 2013: The Community Earth System Model: A Framework for
754 Collaborative Research. *Bulletin of the American Meteorological Society*, **94 (9)**, 1339–1360,
755 https://doi.org/10.1175/BAMS-D-12-00121.1.

756 Jackson, R., and Coauthors, 2021: Holocene polynya dynamics and their interaction with oceanic
757 heat transport in northernmost Baffin Bay. *Scientific Reports*, **11 (1)**, 10 095, https://doi.org/
758 10.1038/s41598-021-88517-9.

759 Jahn, A., and R. Laiho, 2020: Forced Changes in the Arctic Freshwater Budget Emerge in the
760 Early 21st Century. *Geophysical Research Letters*, **47 (15)**, e2020GL088 854, https://doi.org/
761 10.1029/2020GL088854.

762 Jeong, H., S.-S. Lee, H.-S. Park, and A. L. Stewart, 2023a: Future changes in Antarctic coastal
763 polynyas and bottom water formation simulated by a high-resolution coupled model. *Communi-*
764 *cations Earth & Environment*, **4 (1)**, 490, https://doi.org/10.1038/s43247-023-01156-y.

765 Jeong, H., and Coauthors, 2023b: Southern Ocean polynyas and dense water formation in a high-
766 resolution, coupled Earth system model. *The Cryosphere*, **17 (7)**, 2681–2700, https://doi.org/
767 10.5194/tc-17-2681-2023.

768 Kanna, N., S. Sugiyama, Y. Ohashi, D. Sakakibara, Y. Fukamachi, and D. Nomura, 2018: Up-
769 welling of Macronutrients and Dissolved Inorganic Carbon by a Subglacial Freshwater Driven
770 Plume in Bowdoin Fjord, Northwestern Greenland. *Journal of Geophysical Research: Biogeo-*
771 *sciences*, **123 (5)**, 1666–1682, https://doi.org/10.1029/2017JG004248.

772 Kay, J. E., and Coauthors, 2015: The Community Earth System Model (CESM) Large Ensemble
773 Project: A Community Resource for Studying Climate Change in the Presence of Internal Climate
774 Variability. *Bulletin of the American Meteorological Society*, **96 (8)**, 1333–1349, https://doi.org/
775 10.1175/BAMS-D-13-00255.1.

776 Kirillov, S., I. Dmitrenko, D. G. Babb, J. K. Ehn, N. Koldunov, S. Rysgaard, D. Jensen, and
777 D. G. Barber, 2022: The role of oceanic heat flux in reducing thermodynamic ice growth in
778 Nares Strait and promoting earlier collapse of the ice bridge. *Ocean Science*, **18 (5)**, 1535–1557,
779 https://doi.org/10.5194/os-18-1535-2022.

780 Koerner, K. A., A. Limoges, N. Van Nieuwenhove, T. Richerol, G. Massé, and S. Ribeiro, 2021:
781 Late Holocene sea-surface changes in the North Water polynya reveal freshening of northern
782 Baffin Bay in the 21st century. *Global and Planetary Change*, **206**, 103 642, https://doi.org/
783 10.1016/j.gloplacha.2021.103642.

784 Kohnemann, S. H. E., and G. Heinemann, 2025: Gap Flows in Nares Strait: Multi-Scale Numerical
785 Model Simulations in Comparison to Aircraft Measurements. *Earth and Space Science*, **12 (5)**,
786 e2024EA003 912, https://doi.org/10.1029/2024EA003912.

787 Krumhardt, K. M., M. C. Long, Z. T. Sylvester, and C. M. Petrik, 2022: Climate drivers of Southern
788 Ocean phytoplankton community composition and potential impacts on higher trophic levels.
789 *Frontiers in Marine Science*, **9**, https://doi.org/10.3389/fmars.2022.916140.

790 Kwok, R., 2007: Baffin Bay ice drift and export: 2002–2007. *Geophysical Research Letters*,
791 **34 (19)**, https://doi.org/10.1029/2007GL031204.

Kwok, R., L. Toudal Pedersen, P. Gudmandsen, and S. S. Pang, 2010: Large sea ice outflow into the Nares Strait in 2007. *Geophysical Research Letters*, **37 (3)**, https://doi.org/10.1029/2009GL041872.

Laliberté, F., S. E. L. Howell, J.-F. Lemieux, F. Dupont, and J. Lei, 2018: What historical landfast ice observations tell us about projected ice conditions in Arctic archipelagoes and marginal seas under anthropogenic forcing. *The Cryosphere*, **12 (11)**, 3577–3588, https://doi.org/10.5194/tc-12-3577-2018.

Landrum, L. L., A. K. DuVivier, M. M. Holland, K. Krumhardt, and Z. Sylvester, 2024: Defining Antarctic polynyas in satellite observations and climate model output to support ecological climate change research. *EGUsphere*, 1–40, https://doi.org/10.5194/egusphere-2024-3490.

Lemieux, J.-F., F. Dupont, P. Blain, F. Roy, G. C. Smith, and G. M. Flato, 2016: Improving the simulation of landfast ice by combining tensile strength and a parameterization for grounded ridges. *Journal of Geophysical Research: Oceans*, **121 (10)**, 7354–7368, https://doi.org/10.1002/2016JC012006.

Marchese, C., C. Albouy, J.-É. Tremblay, D. Dumont, F. D'Ortenzio, S. Vissault, and S. Bélanger, 2017: Changes in phytoplankton bloom phenology over the North Water (NOW) polynya: a response to changing environmental conditions. *Polar Biology*, **40 (9)**, 1721–1737, https://doi.org/10.1007/s00300-017-2095-2.

Marinov, I., S. C. Doney, and I. D. Lima, 2010: Response of ocean phytoplankton community structure to climate change over the 21st century: partitioning the effects of nutrients, temperature and light. *Biogeosciences*, **7 (12)**, 3941–3959, https://doi.org/10.5194/bg-7-3941-2010.

Meier, W. N., J. S. Stewart, F. Fetterer, and A. K. Windnagel, 2021: NOAA/NSIDC Climate Data Record of Passive Microwave Sea Ice Concentration, Version 4. National Snow and Ice Data Center, https://doi.org/10.7265/efmz-2t65.

Melling, H., Y. Gratton, and G. Ingram, 2001: Ocean circulation within the North Water polynya of Baffin Bay. *Atmosphere-Ocean*, **39 (3)**, 301–325, https://doi.org/10.1080/07055900.2001.9649683.

819 Moore, G. W. K., 2021: Impact of model resolution on the representation of the wind field along
820 Nares Strait. *Scientific Reports*, **11 (1)**, 13 271, https://doi.org/10.1038/s41598-021-92813-9.

821 Moore, G. W. K., S. E. L. Howell, and M. Brady, 2023: Evolving relationship of Nares Strait ice
822 arches on sea ice along the Strait and the North Water, the Arctic's most productive polynya.
823 *Scientific Reports*, **13 (1)**, 9809, https://doi.org/10.1038/s41598-023-36179-0.

824 Moore, G. W. K., S. E. L. Howell, M. Brady, X. Xu, and K. McNeil, 2021: Anomalous collapses
825 of Nares Strait ice arches leads to enhanced export of Arctic sea ice. *Nature Communications*,
826 **12 (1)**, 1, https://doi.org/10.1038/s41467-020-20314-w.

827 Moore, G. W. K., and A. A. Imrit, 2022: Impact of Resolution on the Representation of the
828 Mean and Extreme Winds Along Nares Strait. *Journal of Geophysical Research: Atmospheres*,
829 **127 (19)**, e2022JD037 443, https://doi.org/10.1029/2022JD037443.

830 Moore, G. W. K., and K. Våge, 2018: Impact of model resolution on the representation of the
831 air–sea interaction associated with the North Water Polynya. *Quarterly Journal of the Royal*
832 *Meteorological Society*, **144 (714)**, 1474–1489, https://doi.org/10.1002/qj.3295.

833 Moore, J. K., S. C. Doney, J. A. Kleypas, D. M. Glover, and I. Y. Fung, 2001: An intermediate
834 complexity marine ecosystem model for the global domain. *Deep Sea Research Part II: Topical*
835 *Studies in Oceanography*, **49 (1)**, 403–462, https://doi.org/10.1016/S0967-0645(01)00108-4.

836 Moore, J. K., S. C. Doney, and K. Lindsay, 2004: Upper ocean ecosystem dynamics and iron cycling
837 in a global three-dimensional model. *Global Biogeochemical Cycles*, **18 (4)**, https://doi.org/
838 10.1029/2004GB002220.

839 Moore, J. K., K. Lindsay, S. C. Doney, M. C. Long, and K. Misumi, 2013: Marine Ecosystem
840 Dynamics and Biogeochemical Cycling in the Community Earth System Model [CESM1(BGC)]:
841 Comparison of the 1990s with the 2090s under the RCP4.5 and RCP8.5 Scenarios. *Journal of*
842 *Climate*, **26 (23)**, 9291–9312, https://doi.org/10.1175/JCLI-D-12-00566.1.

843 Mosbech, A., K. L. Johansen, T. A. Davidson, M. Appelt, B. Grønnow, C. Cuyler, P. Lyngs, and
844 J. Flora, 2018: On the crucial importance of a small bird: The ecosystem services of the little
845 auk (Alle alle) population in Northwest Greenland in a long-term perspective. *Ambio*, **47 (2)**,
846 226–243, https://doi.org/10.1007/s13280-018-1035-x.

Muilwijk, M., T. Hattermann, T. Martin, and M. A. Granskog, 2024: Future sea ice weakening amplifies wind-driven trends in surface stress and Arctic Ocean spin-up. *Nature Communications*, **15 (1)**, 6889, https://doi.org/10.1038/s41467-024-50874-0.

Münchow, A., K. K. Falkner, and H. Melling, 2015: Baffin Island and West Greenland Current Systems in northern Baffin Bay. *Progress in Oceanography*, **132**, 305–317, https://doi.org/10.1016/j.pocean.2014.04.001.

Mysak, L. A., and F. Huang, 1992: A Latent-and Sensible-Heat Polynya Model for the North Water, Northern Baffin Bay. *Journal of Physical Oceanography*, **22 (6)**, 596–608, https://doi.org/10.1175/1520-0485(1992)022⟨0596:ALASHP⟩2.0.CO;2.

Noh, K. M., H.-G. Lim, E. J. Yang, and J.-S. Kug, 2023: Emergent Constraint for Future Decline in Arctic Phytoplankton Concentration. *Earth's Future*, **11 (4)**, e2022EF003 427, https://doi.org/10.1029/2022EF003427.

Odate, T., T. Hirawake, S. Kudoh, B. Klein, B. LeBlanc, and M. Fukuchi, 2002: Temporal and spatial patterns in the surface-water biomass of phytoplankton in the North Water. *Deep Sea Research Part II: Topical Studies in Oceanography*, **49 (22)**, 4947–4958, https://doi.org/10.1016/S0967-0645(02)00172-8.

Polyakov, I. V., A. V. Pnyushkov, and E. C. Carmack, 2018: Stability of the arctic halocline: a new indicator of arctic climate change. *Environmental Research Letters*, **13 (12)**, 125 008, https://doi.org/10.1088/1748-9326/aaec1e.

Popova, E. E., and Coauthors, 2012: What controls primary production in the Arctic Ocean? Results from an intercomparison of five general circulation models with biogeochemistry. *Journal of Geophysical Research: Oceans*, **117 (C8)**, https://doi.org/10.1029/2011JC007112.

Preußer, A., G. Heinemann, S. Willmes, and S. Paul, 2015: Multi-Decadal Variability of Polynya Characteristics and Ice Production in the North Water Polynya by Means of Passive Microwave and Thermal Infrared Satellite Imagery. *Remote Sensing*, **7 (12)**, 15 844–15 867, https://doi.org/10.3390/rs71215807.

Raghavan, M., and Coauthors, 2014: The genetic prehistory of the New World Arctic. *Science (New York, N.Y.)*, **345 (6200)**, 1255 832, https://doi.org/10.1126/science.1255832.

Rasmussen, T. A. S., N. Kliem, and E. Kaas, 2011: The Effect of Climate Change on the Sea Ice and Hydrography in Nares Strait. *Atmosphere-Ocean*, **49 (3)**, 245–258, https://doi.org/10.1080/07055900.2011.604404.

Ren, H., M. Shokr, X. Li, Z. Zhang, F. Hui, and X. Cheng, 2022: Estimation of Sea Ice Production in the North Water Polynya Based on Ice Arch Duration in Winter During 2006–2019. *Journal of Geophysical Research: Oceans*, **127 (10)**, e2022JC018 764, https://doi.org/10.1029/2022JC018764.

Ribeiro, S., and Coauthors, 2021: Vulnerability of the North Water ecosystem to climate change. *Nature Communications*, **12 (1)**, 4475, https://doi.org/10.1038/s41467-021-24742-0.

Sanderson, B. M., and Coauthors, 2017: Community climate simulations to assess avoided impacts in 1.5 and 2 °C futures. *Earth System Dynamics*, **8 (3)**, 827–847, https://doi.org/10.5194/esd-8-827-2017.

Schmidt, S., and U. Send, 2007: Origin and Composition of Seasonal Labrador Sea Freshwater. *Journal of Physical Oceanography*, **37 (6)**, 1445–1454, https://doi.org/10.1175/JPO3065.1.

Séférian, R., and Coauthors, 2020: Tracking Improvement in Simulated Marine Biogeochemistry Between CMIP5 and CMIP6. *Current Climate Change Reports*, **6 (3)**, 95–119, https://doi.org/10.1007/s40641-020-00160-0.

Sterlin, J., T. Orval, J.-F. Lemieux, C. Rousset, T. Fichefet, F. Massonnet, and J. Raulier, 2024: Influence of the representation of landfast ice on the simulation of the Arctic sea ice and Arctic Ocean halocline. *Ocean Dynamics*, **74 (5)**, 407–437, https://doi.org/10.1007/s10236-024-01611-0.

Stock, C. A., and Coauthors, 2017: Reconciling fisheries catch and ocean productivity. *Proceedings of the National Academy of Sciences*, **114 (8)**, E1441–E1449, https://doi.org/10.1073/pnas.1610238114.

Stroeve, J., and D. Notz, 2018: Changing state of Arctic sea ice across all seasons. *Environmental Research Letters*, **13 (10)**, 103 001, https://doi.org/10.1088/1748-9326/aade56.

Tamura, T., and K. I. Ohshima, 2011: Mapping of sea ice production in the Arctic coastal polynyas. *Journal of Geophysical Research: Oceans*, **116 (C7)**, https://doi.org/10.1029/2010JC006586.

Tang, C. C., C. K. Ross, T. Yao, B. Petrie, B. M. DeTracey, and E. Dunlap, 2004: The circulation, water masses and sea-ice of Baffin Bay. *Progress in Oceanography*, **63 (4)**, 183–228, https://doi.org/10.1016/j.pocean.2004.09.005.

Tremblay, J.-É., Y. Gratton, E. C. Carmack, C. D. Payne, and N. M. Price, 2002: Impact of the large-scale Arctic circulation and the North Water Polynya on nutrient inventories in Baffin Bay. *Journal of Geophysical Research: Oceans*, **107 (C8)**, 26–1–26–14, https://doi.org/10.1029/2000JC000595.

Vancoppenolle, M., L. Bopp, G. Madec, J. Dunne, T. Ilyina, P. R. Halloran, and N. Steiner, 2013: Future Arctic Ocean primary productivity from CMIP5 simulations: Uncertain outcome, but consistent mechanisms. *Global Biogeochemical Cycles*, **27 (3)**, 605–619, https://doi.org/10.1002/gbc.20055.

Vincent, R. F., 2019: A Study of the North Water Polynya Ice Arch using Four Decades of Satellite Data. *Scientific Reports*, **9 (1)**, 20 278, https://doi.org/10.1038/s41598-019-56780-6.

Vincent, R. F., 2020: An Examination of the Non-Formation of the North Water Polynya Ice Arch. *Remote Sensing*, **12 (17)**, 2712, https://doi.org/10.3390/rs12172712.

Wolf, K. K. E., C. J. M. Hoppe, L. Rehder, E. Schaum, U. John, and B. Rost, 2024: Heatwave responses of Arctic phytoplankton communities are driven by combined impacts of warming and cooling. *Science Advances*, **10 (20)**, eadl5904, https://doi.org/10.1126/sciadv.adl5904.

Yao, T., and C. L. Tang, 2003: The formation and maintenance of the North Water Polynya. *Atmosphere-Ocean*, **41 (3)**, 187–201, https://doi.org/10.3137/ao.410301.

Zanowski, H., A. Jahn, and M. M. Holland, 2021: Arctic Ocean Freshwater in CMIP6 Ensembles: Declining Sea Ice, Increasing Ocean Storage and Export. *Journal of Geophysical Research: Oceans*, **126 (4)**, e2020JC016 930, https://doi.org/10.1029/2020JC016930.

Supplementary figures to: Future Sea Ice-Ocean and Biological Productivity Changes in the North Water Polynya Region under Policy Relevant Warming Levels

Jed Lenetsky[1], Alexandra Jahn[1], Patrick Ugrinow[1], Christopher Wyburn-Powell[1], Rajan Patel[1], and Hannah Zanowski[2]

[1]Department of Atmospheric and Oceanic Sciences and Institute of Arctic and Alpine Research, University of Colorado - Boulder, Boulder, Colorado, USA

[2]Department of Atmospheric and Oceanic Sciences, University of Wisconsin-Madison, Madison, Wisconsin, USA

October 12, 2025

Warming Level	Mean	Maximum	Minimum
LOW	1.95°C	2.04°C	1.88°
HIGH	4.22°C	4.89°C	3.52°

Table S1: 30 year ensemble mean, ensemble maximum, and ensemble minimum global temperature anomalies for LOW and HIGH.

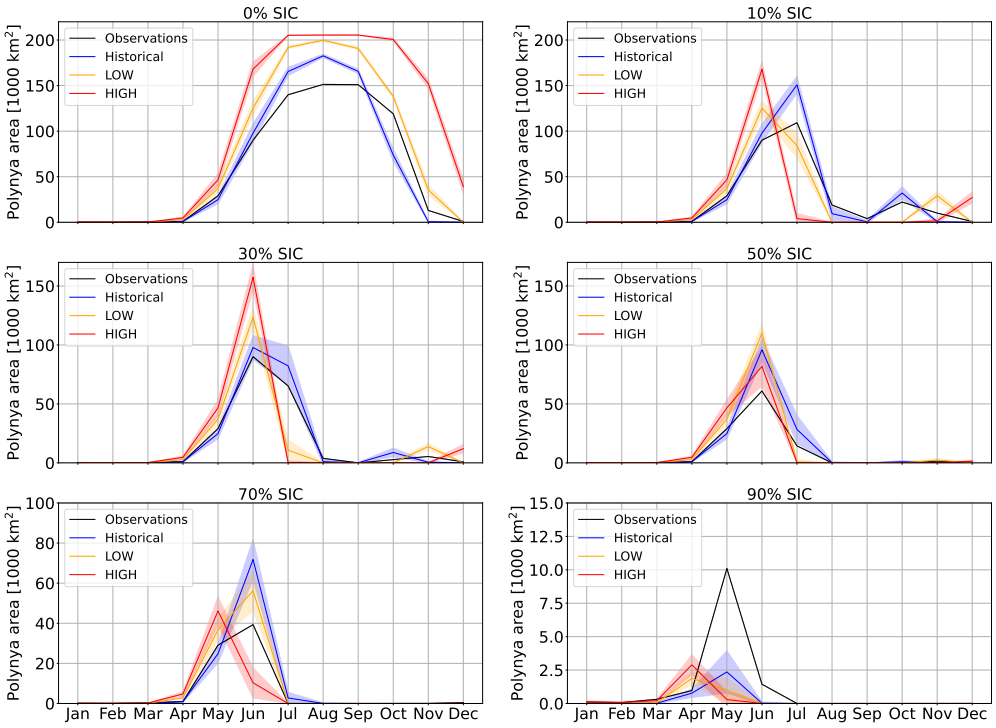

Figure S1: Influence of the SIC threshold choice for when the NOW polynya ceases to exist due to becoming part of Baffin Bay open water (using the southern box shown in Fig. 3) on the seasonal cycle of the polynya for observations (1980-2009; black), CESM1-LE historical (1980-2009; blue), LOW (orange), and HIGH (red). Shading indicates ± 1-standard deviation from the ensemble mean. Note the different y axis limits.

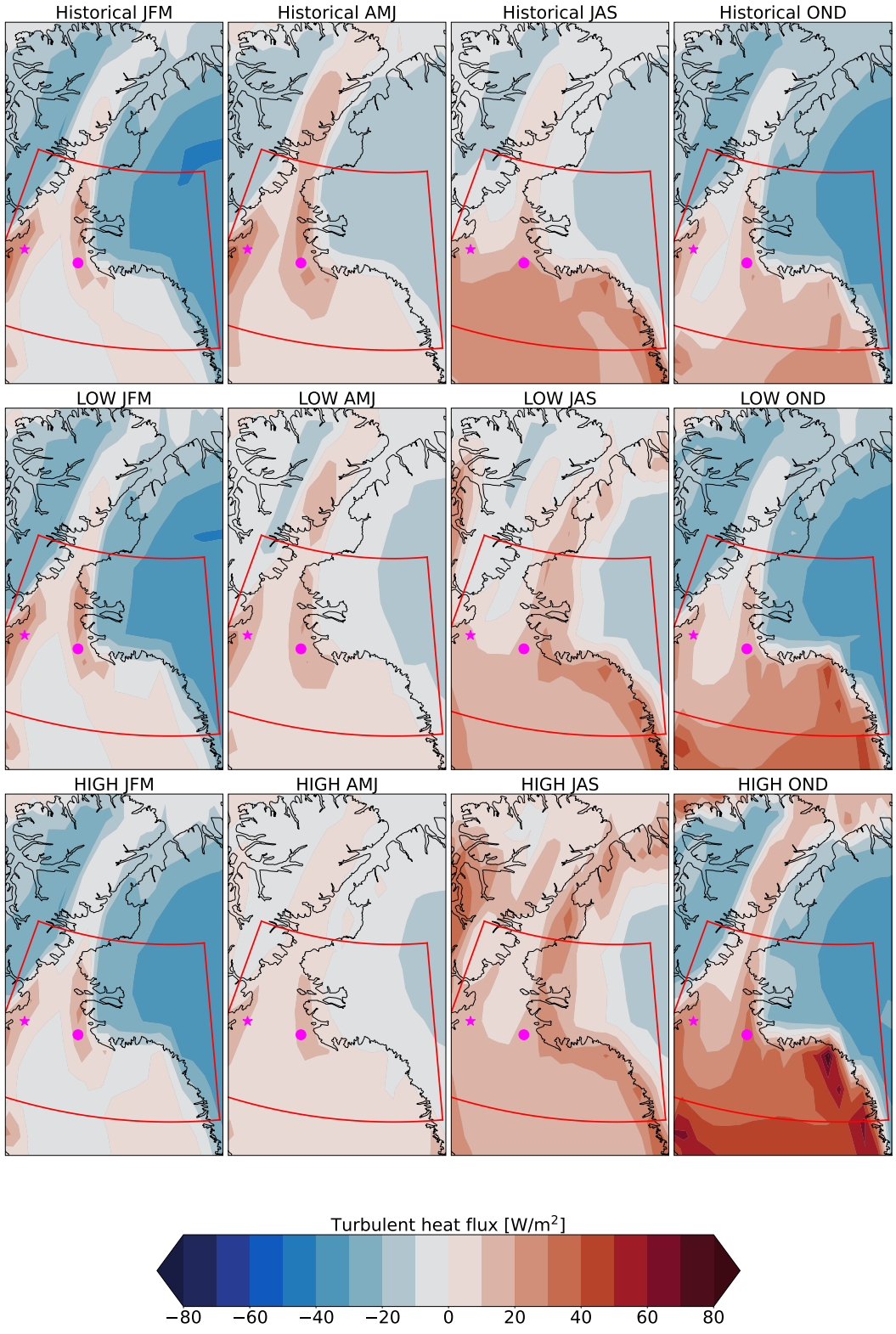

Figure S2: Seasonal cycle of turbulent heat fluxes (latent + sensible) over the NOW region (red box) during the CESM1-LE historical period (1980-2009), LOW, and HIGH for winter (JFM), spring (AMJ), summer (JAS) and fall (OND). Positive fluxes are atmospheric heat gain. The location of the east and west points used for NPP assessment in Fig. 12 are shown as a black star and circle respectively.

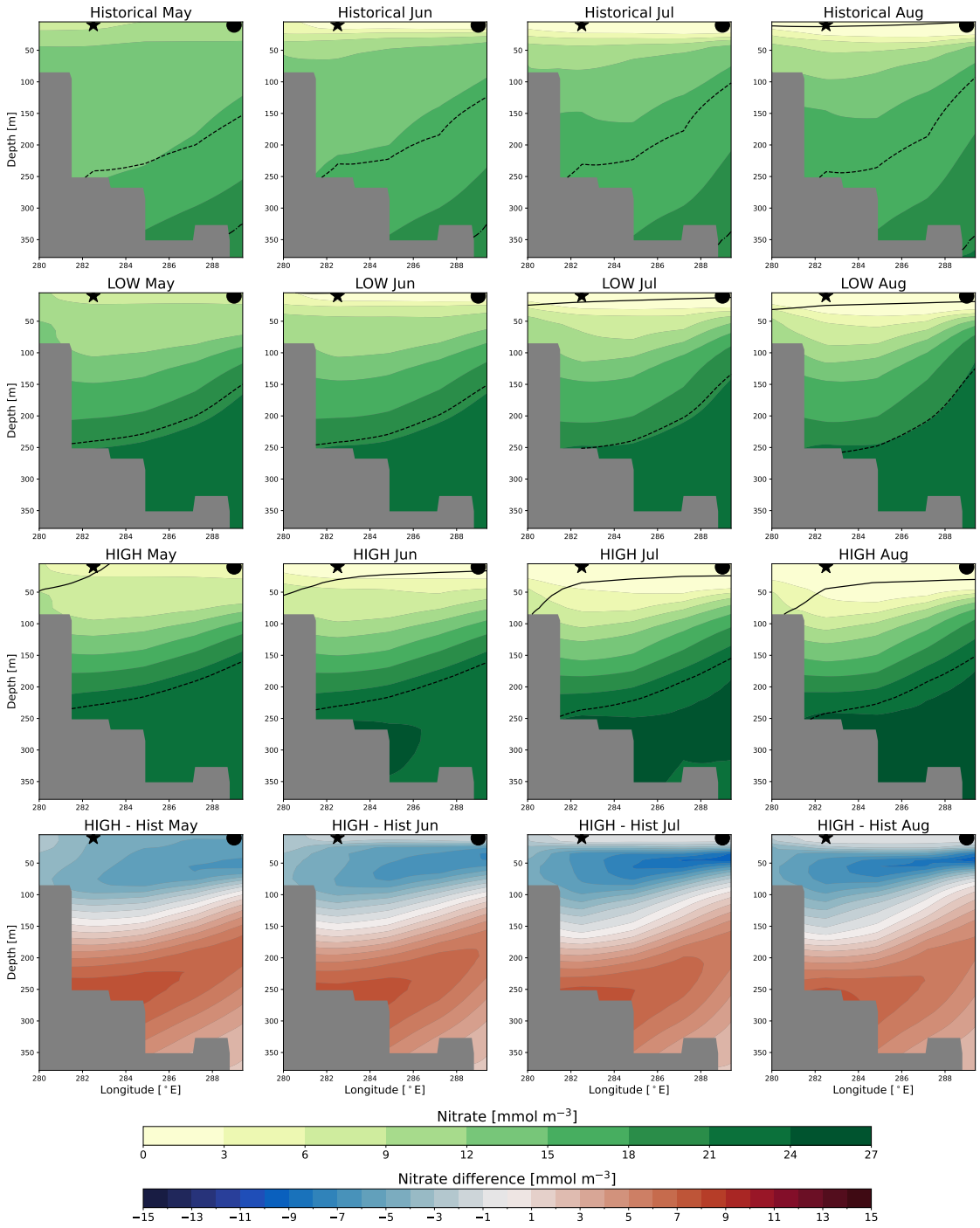

Figure S3: Cross section of Nitrate (NO_3^-) concentration along 76.2 °N across the NOW region (see Fig. 2 or 11 for the location of the section) for May through August historical, LOW, and High. The 25.0, 27.0, and 27.5 σ_θ isopycnals are shown in solid, dashed, and dash-dotted black lines respectively. The bottom row shows the difference between HIGH and the historical period. The location of the east and west points used for NPP assessment in Fig. 12 are shown as a black star and circle respectively.

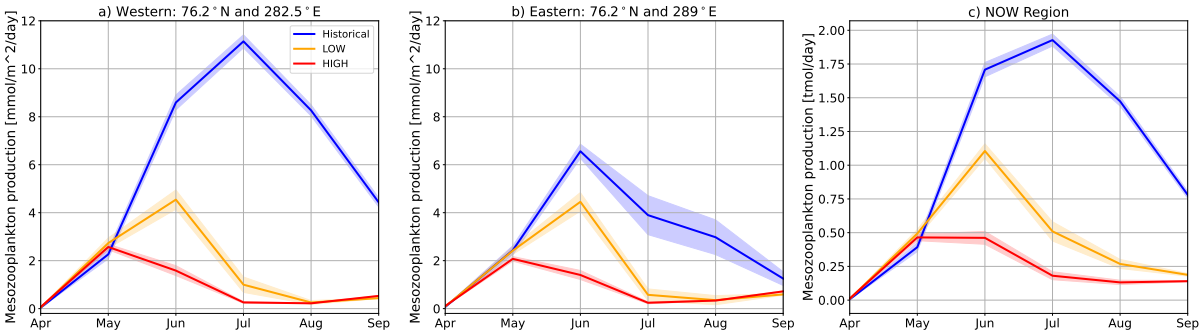

Figure S4: Seasonal cycle of mesozooplankton production during the a) CESM1-LE historical period (1980-2009), and b) LOW, and c) HIGH. Shading indicates ± 1-standard deviation from the ensemble mean.

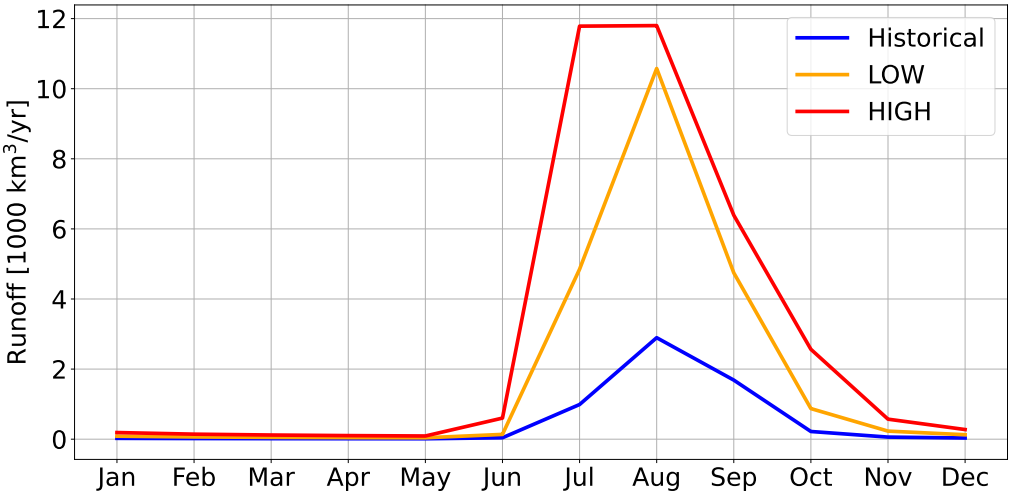

Figure S5: Seasonal cycle of total simulated runoff into the NOW domain (see Fig. 3) for historical (blue), LOW (orange), and HIGH (red).